School of Mechanical and Manufacturing Engineering

Faculty of Engineering

UNSW Sydney

BY

Fernan Bautista

3D PRINTING REALISTIC CORONARY ARTERIAL REPLICAS

Thesis submitted as a requirement for the degree of Master of Engineering (Mechanical Engineering)

Submitted: 22 November 2019

Student zID: z5167369

Supervisor: Susann Beier (UNSW)

ORIGINALITY STATEMENT

'I hereby declare that this submission is my own work and to the best of my knowledge it contains no materials previously published or written by another person, or substantial proportions of material which have been accepted for the award of any other degree or diploma at UNSW or any other educational institution, except where due acknowledgement is made in the thesis. Any contribution made to the research by others, with whom I have worked at UNSW or elsewhere, is explicitly acknowledged in the thesis. I also declare that the intellectual content of this thesis is the product of my own work, except to the extent that assistance from others in the project's design and conception or in style, presentation and linguistic expression is acknowledged.'

Signed __Fernan Bautista ______

Date __22 November 2019____

Abstract

Coronary artery disease, causing fatal heart attacks is the leading cause of death in the world. Experiments are necessary for studies to combat this widespread disease; however, due to patient variability among several concerns, there's a lack of accurate representation of arterial shapes and tissue properties. This report explores studies on methods and limitations to replicate the mechanical properties of the coronary artery with the aid of a Polyjet 3D printer (Projet MJP 5600) and computer simulations. Analysis are made to show that there is potential to develop mechanically realistic arterial properties using a dual metamaterial structure design.

Acknowledgements

I would like to briefly thank the following especially for the help they have provided me to understand more about the coronary artery disease, methods to replicate the coronary arteries and laboratory processes such as the use of the tensile machine and 3D printers. Dr. Susann Beier(supervisor); Dr. Blake Cochran(consultation); Terry Flynn (lab consultation); Lynn Ferris(consultation); Somesh Khullar; and Seetha Mahadevan (lab consultation).

Contents

List of figures

List of tables

Nomenclature

σ	=	Stress
ε	=	Strain
λ	=	Wavelength
A	=	Amplitude
r	=	Radius

I. Introduction

This report introduces the general knowledge and progress of the research regarding the attempt of replicating realistic coronary arterial phantoms. General information regarding cardiovascular disease and coronary artery disease in particular is outlined such as the statistics, detection or diagnosis methods, and treatment methods. General information regarding 3D printing and methods of phantom replication is also provided such as the different types of 3D printing or additive manufacturing, its advantages and disadvantages among many others.

1. Cardiovascular Disease (CVD)

Cardiovascular disease is the leading cause of death in the world. It was estimated to have caused 17.9 million people's deaths as it represented around 31% of all the deaths globally in 2016 [1]. CVD in Australia alone has caused around 18,590 deaths in 2017 [2]. There is therefore a need to put more effort to understand the causes, effects and treatment by conducting more studies, research and development.

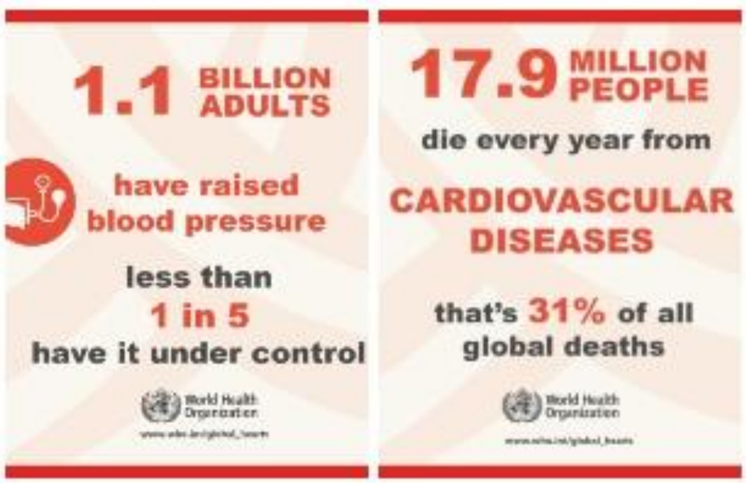

Figure 1. Graphical representation of CVD statistics [3]

CVDs often lead to heart attacks and strokes which are the events that mainly cause a blockage in the blood vessels. With the build-up of fatty deposits or cholesterol in the blood on the inner walls of the vessel, it prevents blood supply to the heart or brain which may be very lethal [1]. There are many different types of CVD and many different combinations and factors that may lead to the development of the disease.

2. Coronary Artery Disease (CAD)

The most common type of cardiovascular disease is the coronary artery disease [4]. CAD is the disease of the blood vessels that reduces the blood flow to the heart and is the main cause of heart attacks. The main underlying event that causes this disease is called atherosclerosis [5].

Atherosclerosis is wherein the inside of an artery narrows due to the build-up of a fatty material called plaque. [5] This build up happens over a long period of time as can be seen from Figure 2.

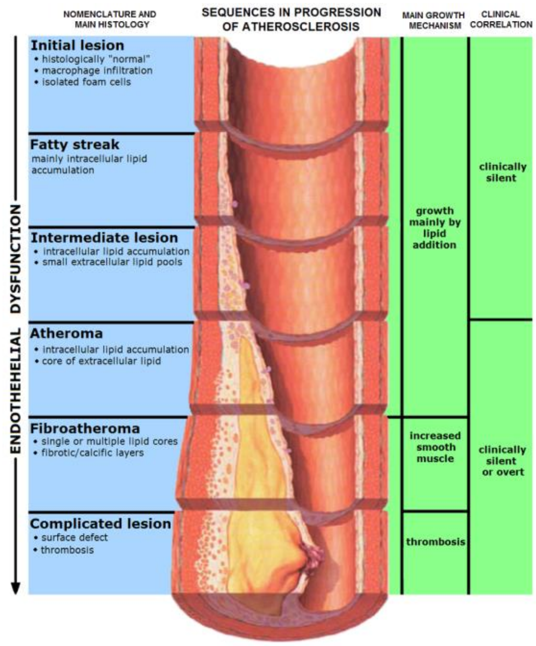

Figure 2. Atherosclerosis development [6]

Diagnosis can be done through different methods such as electrocardiogram (ECG), coronary angiogram or coronary computed tomography angiogram (CCTA), echocardiogram (heart ultrasound), blood tests, myocardial perfusion study, intravascular ultrasound (IVUS) and others [7]. These tests to detect the disease will help the doctors decide the best type of treatments according to their findings.

Treatment for coronary artery disease usually involves lifestyle changes and, if necessary, drugs and certain medical procedures depending on the stage of the disease. While the lifestyle changes and medication may be enough for the early stages of the stages, if the disease has already developed onto the later stages, angioplasty stent placement or coronary artery bypass surgery are two of the most common ways to treat the disease [8].

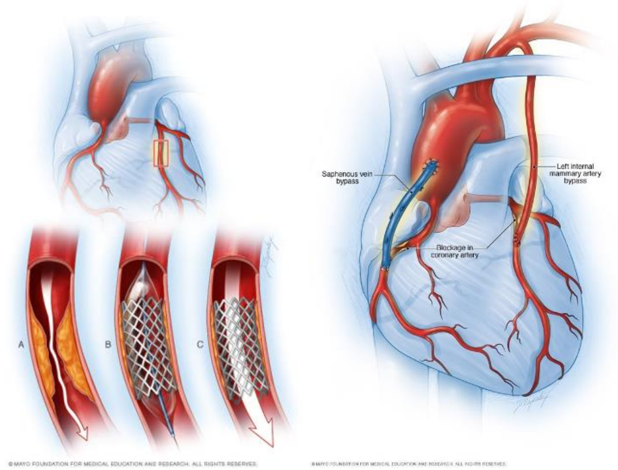

Figure 3. Stent placement and coronary artery bypass [8]

3. Arterial Replicas

To combat this disease, an area of research for understanding it is the hemodynamic assessments in the coronary which is the study of blood flow. To study the blood flow, simulations are conducted in different ways such with the use of computer aided design and engineering as well as experimental setups involving the use of phantoms.

Medical models, or "phantoms," have been widely used for medical training and for doctor-patient interactions. They are increasingly used for surgical planning, medical computational models, algorithm verification and validation, and medical devices development. There are a multitude of methods to manufacture these phantoms. Among these methods is 3D printing. Several techniques and research have been done that has applied these recently developed technology in the medical field.

II. Literature Review

This section provides a review of the related literature regarding 3D printing advancements and applications in the medical field along with the different additive manufacturing methods and materials. This section also provides a review on different studies conducted by different researchers regarding the mechanical properties of the arterial vessels as well as the disease and possible locations of the disease.

1. Phantom manufacturing methods & Geometry

The common advantage and disadvantage to be generally understood when using phantoms to conduct studies for hemodynamic analysis are the following:

- Main advantage is it being a non-invasive tool for conducting medical experiments.

- Main disadvantage is plenty of assumptions are made that may inaccurately represent in vivo effects.

To reduce the identified disadvantages in using phantoms, it would be then be beneficial to attempt to make more realistic phantoms.

Most medical phantoms of blood vessels have often been manufactured using either PDMS, 3D printing or a combination of these. There are multiple methods of 3D printing that has currently been developed in the industry. 3D printing technology has rapidly aided the development of lower cost and more complex phantoms. These phantoms have increasingly been more realistic as more developments have also been made in imaging devices such as computer tomography (CT) among many other methods of detecting and scanning the vascular system [9]. Despite the developments however, there are still limitations regarding the quality of 3D printing and there are also still limited materials available for printing that can replicate all tissue properties.

One of the phantom fabrication methods that have been applied to more accurately mimic mechanical properties of the artery is by constructing the geometry with the 3 layers namely the intima, media and adventitia and matching the thickness and layer properties to real tissue properties evaluated from related literature [10]. This article however did not specifically mention the properties and geometry details used.

Some 3D printers especially more sophisticated and advanced models are capable of fabricating phantoms that can be accurate up to the micron level. Most of the printers typically use polymeric materials that can be designed to match the properties and mechanical behaviour of real tissues [11]. While it is certainly possible to match some of the properties of the polymer to the soft tissue, it can be observed from Figure 4 that it cannot entirely match the properties for the entirety of the loading conditions until failure. Experiments to test the mechanical behaviour of the polymer and related literature is therefore necessary to identify how much of the loading conditions is relevant to the study.

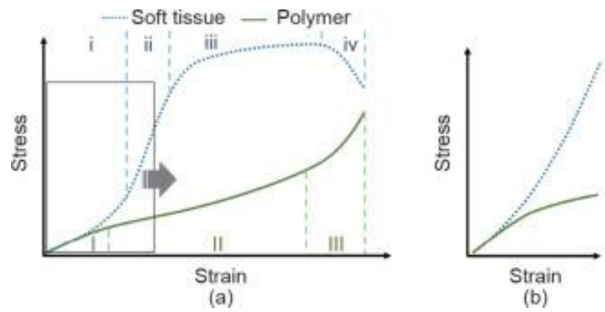

Figure 4. Comparison of mechanical behavior of soft tissue and polymer [11]

Since it is difficult to find materials, specifically polymeric or multi-materials, that have an available stress-strain curve, it will be necessary to print the material with different properties and then evaluate the behaviour to figure out which type of material would match the behaviour of the tissue. For the related literature regarding the properties of the blood vessel tissue, it will be provided in section II.B of this report.

Another method to mimic the soft tissue properties is of a technique of specifically altering the properties of a produced part which has been done through the use of metamaterials [11]. This is an artificially structured material that can be shaped into different geometrical arrangements as shown in Figure 5. This can then result to different mechanical behaviours such as shown in Figure 6.

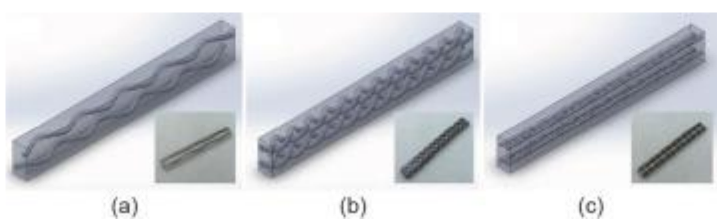

Figure 5. Different metamaterial shapes. (a) sinusoidal wave design, (b) double helix design, and (c) interlocking chain design [11]

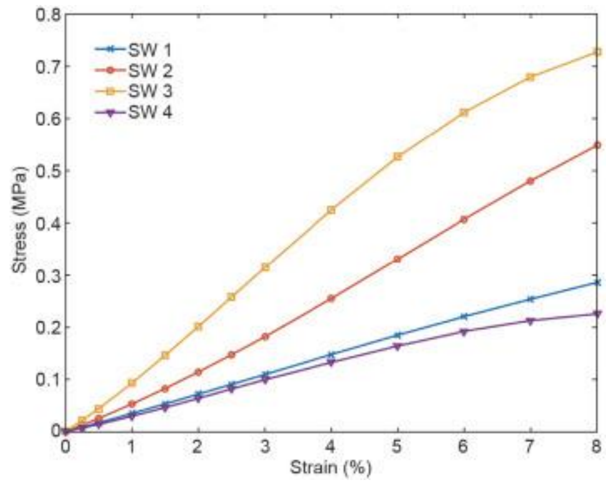

Figure 6. Stress-strain curve based on different metamaterials [11]

No studies however have currently been found using this method of metamaterials construction for coronary arterial arteries.

There are multiple types of 3D printers available in the market right now. For UNSW, a multi-material polyjet 3D printer is available that can produce highly accurate prints (Layer thickness of 13µ and accuracy of 0.05mm per 25.4mm) [12]. Polyjet 3D printing technology works similar to how an inkjet printer works. This printer jets drops of photopolymer that would solidify when it is exposed to UV light. This results to faster build times and more accurate prints while even capable of printing multiple materials at the same time [13].

Despite the numerous benefits and numerous applications of 3D printing today, a known fact that often results from 3D printing is the anisotropic properties that results from this type of manufacturing. This is a challenge that the additive manufacturing industry has been taking into account [14]. Different parameters such as the printer type, printing orientation, print speeds, temperature, nozzle or layer thickness, or density among many are therefore needed to be considered when using 3D printing to manufacture parts that require very specific mechanical properties.

In recent years, most phantoms are made with either silicone or rigid plastics made from 3D printing. This is from the assumption that there are minimal effects on the hemodynamic flow in the arteries. However, the potential effects of material elasticity in the cellular level as well as disease development is unknown.

2. Arterial and Plaque (disease) Properties

To be able to mimic the properties of the coronary arteries, knowing what those properties are in the first place are necessary. Among the coronary arteries, the left anterior descending (LAD) is of central importance in the circulatory pathophysiology. Stenting is most often or more commonly happening in the LAD that at most other coronary locations [15]. In a study by Holzapfel et al., a test to determine the mechanical properties of the different layers of the human coronary arteries were done on several patients as shown on Figure 7.

	Specimen No.												
	I	*II*	*III*	*IV*	*V*	*VI*	*VII*	*VIII*	*IX*	*X*	*XI*	*XII*	*XIII*
Age, yr	80	73	80	64	73	75	73	75	72	77	69	64	54
Gender	F	M	F	F	M	M	M	M	M	M	M	M	M
Primary disease	PT	HC	PN	CK	PC	PN	CC	PC	LC	DE	HT	SA	BC
Cause of death	PAE	GHD	GHD	UR	IL	GHD	MOF	GHD	PN	PN	AP	AP	GHD
	Atherosclerosis												
Aorta	√	√	√	√	√	√	√	√	√	√	−	√	√
Coronary arteries	√	−	−	√	√	√	√	√	√	√	−	−	−
Cerebral arteries	−	−	−	−	√	√	−	√	−	−	−	√	−
Renal arteries	√	−	−	√	−	−	−	−	−	√	√	−	√

M, male; F, female; AP, apoplexy; BC, bronchus carcinoma; CC, colon carcinoma; CK, polycystic kidney disease; DE, dementia; GHD, global heart dilation; HC, hydrocephalus internus with tetraparesis; HT, hypertension; IL, ileus; LC, liver carcinoma; MOF, multiple organ failure; PAE, pulmonary artery embolism; PC, pancreas carcinoma; PN, pneumonia; PT, phlebothrombosis of the leg; SA, salmonellosis; UR, uremia. Assessment of atherosclerosis is based on autopsy reports: √, medium- or high-grade atherosclerosis; −, no or low-grade atherosclerosis.

Figure 7. Anamnesis of patients for a study on determining mechanical properties of layer-specific coronary arteries [15]

The data from this study indicate there also not much correlation between the time period from death to the mechanical testing to the tissue properties. This has been hypothesised since the tissues are bradytrophic which meant that there is a delay for several days before the proteolytic activity where tissue cell breakdown occurs. The study indicated as well that there is significant correlation between the patient's age and the stretch properties as it showed that the axial *in situ* stretch decreases with age. All three tissue types, namely the adventitia, media and intima, exhibit an anisotropic and nonlinear mechanical behaviours. [15] The properties are as shown in Figure 8 and Figure 9.

	Arterial Layer and Orientation					
	Adventitia		Media		Intima	
	AC (n = 5)	AL (n = 6)	MC (n = 9)	ML (n = 7)	IC (n = 6)	IL (n = 7)
$\bar{\sigma}_{ult}$, kPa	1430.0±604.0	1300.0±692.0	446.0±194.0	419.0±188.0	394.0±223.0	391.0±144.0
$\bar{\lambda}_{ult}$	1.66±0.24	1.87±0.38	1.81±0.37	1.74±0.28	1.60±0.29	1.55±0.40

Values are means ± SD; n, number of specimens, which fractured in the gauge region. $\bar{\sigma}_{ult}$, Ultimate tensile stress; $\bar{\lambda}_{ult}$, ultimate stretch; AC and AL, circumferential and longitudinal adventitia; MC and ML, circumferential and longitudinal media; IC and IL, circumferential and longitudinal intima.

Figure 8. Mechanical properties of the arterial layers from Figure 7 [15]

As mentioned in the previous section of the report, some of the behaviour of the material can be mimicked through different means however it is still unknown whether the 3d printed material will exhibit the same stretch behaviour as from the literature.

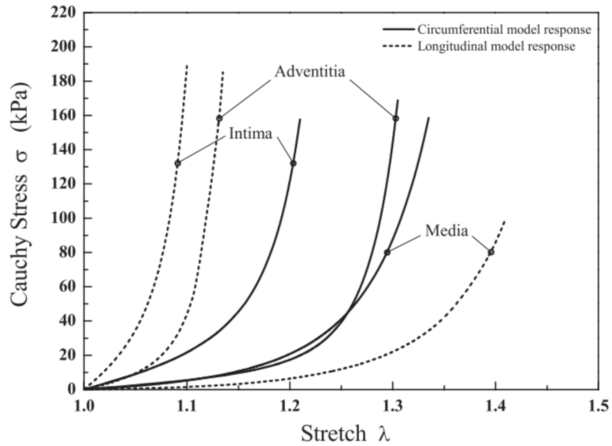

Figure 9. Cauchy Stress-Stretch curve of different arterial layers [15]

Despite this information, a limitation that this study has is that the structural integrity of the strips may have been disturbed during the handling and preparation. This could have altered the mechanical properties of the sample tissue during the cutting for example. Another possible limitation to this study is the relatively small amount of sample tissue specimens that were investigated. More data from other sources may then be needed to be able to have a more comprehensive comparison.

As the previous data provides both the behaviour from the curve and the ultimate stresses, we can only use the ultimate stresses as initial comparison to available material data from the prospective 3D printer to be used. Figure 10 below shows which multi-material combination may then be used for initial testing.

PROPERTIES	ASTM	MULTI-MATERIAL COMPOSITES (VisiJet CR-CL 200** + VisiJet CE-NT)										
Material Name		RCL-ENT-D75	RCL-ENT-D70	RCL-ENT-D65	RCL-ENT-D60	RCL-ENT-D55	RCL-ENT-A90	RCL-ENT-A80	RCL-ENT-A70	RCL-ENT-A60	RCL-ENT-A50	RCL-ENT-A40
Description		Very rigid	Slightly rigid	Rigid	Rigid	Slightly rigid	Slightly flexible	Slightly flexible	Flexible	Flexible	More flexible	Very flexible
Appearance*		Very clear white	Light clear white	Light clear white	Light clear tan	Light clear tan	Medium clear tan	Medium clear tan	Medium clear tan	Translucent tan	Translucent amber	Translucent amber
Tensile Strength (MPa)	D638	19-27	12-16	8-10	4-5	2-3	1.4-1.9	1.3-1.7	.75-1.1	.48-.77	.35-.48	.23-.32
Flexural Strength (MPa)	D790	18-21	12-13	7-7.4	3.9-4.2	1.6-1.9	N/A	N/A	N/A	N/A	N/A	N/A
Flexural Modulus (MPa)	D790	450-750	350-550	150-250	70-180	30-80	N/A	N/A	N/A	N/A	N/A	N/A
Impact Strength (J/m) (Notched Izod)	D256	18-25	22-30	32-52	29-42	74-114	N/A	N/A	N/A	N/A	N/A	N/A
Shore A Hardness, Scale A	D2240	N/A	N/A	N/A	N/A	N/A	86-92	75-85	65-75	55-65	45-55	35-45
Shore D Hardness, Scale D	D2240	70-80	65-75	60-70	55-65	50-60	N/A	N/A	N/A	N/A	N/A	N/A
Tear Resistance (kN/m)	D624	N/A	N/A	N/A	N/A	N/A	44-62	25-32	18-23	11-17	6.6-9.3	6.5-8.5

*Visual approximation. No guarantee that part output will match exactly to software or datasheet values.
** Respectively replaces former VisiJet® CR-WT and VisiJet® CR-CL

Figure 10. Projet MJP 5600 materials with similar strength properties from Figure 8 [12]

Another study from Holzapfel et al, included the properties of the coronary vessels that took into consideration the properties with the disease and are shown in Figure 11 and Figure 12.

Anamnesis: CIA, common iliac artery; EIA, external iliac artery; IIA, internal iliac artery; AH, antihypertensives; AS, atherosclerosis; BP, bronchopneumonia; BS, bypass surgery; CS, coronary sclerosis; GHD, global heart dilation; GS, generally atherosclerosis; MI, myocardial infarction. Types of atherosclerotic lesions are according to Stary et al. Assessment of atherosclerosis is based on autopsy reports (y, medium or high grade; n, no or low grade).

Specimen Type of iliac artery	I EIA	II CIA	III IIA	IV CIA	V CIA	VI IIA	VII CIA	VIII IIA	IX CIA
Age (yrs)	65	90	80	64	81	60	60	87	87
Sex	f	m	f	f	f	m	m	f	f
Primary disease	CS	GS	AS	CS	CS	CS	AS	GS	GS
Cause of death	MI	MI	BP	MI	MI	GHD	MI	BP	BP
Atherosclerosis									
Type of atherosclerotic lesions	*V*	*VII*	*V*	*VIII*	*VII*	*VII*	*VII*	*VII*	*VIII*
Adjoining vessels	y	y	y	y	y	n	y	y	y
Peripheral	y	y	y	y	y	n	y	y	y
Coronary	y	y	y	y	y	y	y	y	y
Cerebral	y	y	n	n	y	n	n	y	y
Renal	y	y	y	n	y	n	n	y	y
Cardiovascular treatments	n	AH	n	BS	n	n	n	n	n

Figure 11. Anamnesis of patients for a study on properties of coronary arteries with disease [16]

		Tissue type											
		A		M-nos		I-nos		I-fc		I-fm		M-f	
Specimen		*c*	*a*	*c*	*a*	*c*	*a*	*c*	*a*	*c*	*a*	*c*	*a*
I	σ_{ult}	618.5	737.6	261.5	183.7			205.6	509.8		171.8	1278.1	181.5
	λ_{ult}	1.243	1.223	1.156	1.863			1.374	1.121		1.135	1.076	1.797
II	σ_{ult}	832.3	667.6	212.9	128.4	435.2	1321.9	299.3	617.5				
	λ_{ult}	1.173	1.392	1.409	2.005	1.129	1.117	1.073	1.068				
III	σ_{ult}	1188.3	1276.6	229.7	261.6			126.4			366.5		
	λ_{ult}	1.479	1.157	1.249	1.169			1.232			1.071		
IV	σ_{ult}	845.4	886.6	201.6				292.2					
	λ_{ult}	1.424	1.299	1.280				1.213					
V	σ_{ult}		990.7		432.7	356.4		301.3		941.1	294.3		
	λ_{ult}		1.282		1.830	1.201		1.076		1.071	1.057		
VI	σ_{ult}	802.3		298.2	121.8			287.9	506.1	999.2			
	λ_{ult}	1.413		1.177	1.283			1.126	1.058	1.078			
VII	σ_{ult}	1479.5		108.9	92.5	473.9	796.2	360.1	449.2	390.1		869.0	
	λ_{ult}	1.676		1.323	1.284	1.320	1.159	1.138	1.232	1.173		1.154	
VIII	σ_{ult}	1090.1	1005.3	93.7	141.3	368.2	703.8		402.3				193.2
	λ_{ult}	1.458	1.458	1.260	1.583	1.648	1.435		1.121				1.176
IX	σ_{ult}	1396	1097.9	209.9	148.1	809.1	952.9	165.8	326.9				
	λ_{ult}	1.652	1.658	1.313	1.267	1.357	1.309	1.222	1.208				
mean	$\bar{\sigma}_{ult}$	1031.6	951.8	202.0	188.8	488.6	943.7	254.8	468.6	776.8	277.5	1073.6	187.4
SD		306.8	209.0	69.8	110.9	185.6	272.3	79.8	100.1	336.2	98.4	289.3	8.3
mean	$\bar{\lambda}_{ult}$	1.440	1.353	1.270	1.536	1.331	1.255	1.182	1.135	1.107	1.088	1.115	1.487
SD		0.175	0.168	0.081	0.327	0.199	0.146	0.100	0.071	0.057	0.042	0.055	0.439

Figure 12. Stress and stretch properties of tissue specimens from Figure 11 [16]

In atherosclerosis, it has been known that the main trigger that causes fatal heart attacks and the like are not from the plaque itself but from the rupture of the plaque's fibrous caps [17]. In some early biomechanical analyses that has used finite element analysis, it has been showed that the thin fibrous caps are susceptible to rupture at a peak stress of threshold less than 300kPa. However, in more recent studies it was argued that the rupture of the fibrous caps occurs far lower than the 300kPa threshold for fibrous cap with a thickness of >100μm [18]. Another study has indicated the use of a neo-Hookean material model to for the vessel wall and lipid pool components, with a shear moduli of 200 and 0.5 kPa, respectively [19].

In order to attain more data, studies from other blood vessels such as the carotid were also investigated. From a study of mechanical properties of carotid plaque fibrous caps, a measured indentation response was used to determine elastic properties of the tissue material. It was found that the shear modulus was from a range of 7-100 kPa wherein the medial value was around 11 kPa [20]. In a study done by Chai, C. K., an indentation method was applied to test and measure the properties of a human atherosclerotic carotid plaque caps. The results showed measurements of a median of 14.9MPa wherein the 25th percentile to the 75th percentile data was within 5.6MPa to 54.4MPa for ultimate stresses. In the same study it also showed a single plaque to have a measured young's moduli from a range of 6kPa to 891kPa [21]. This shows that there is a very wide range of materials data for human tissues.

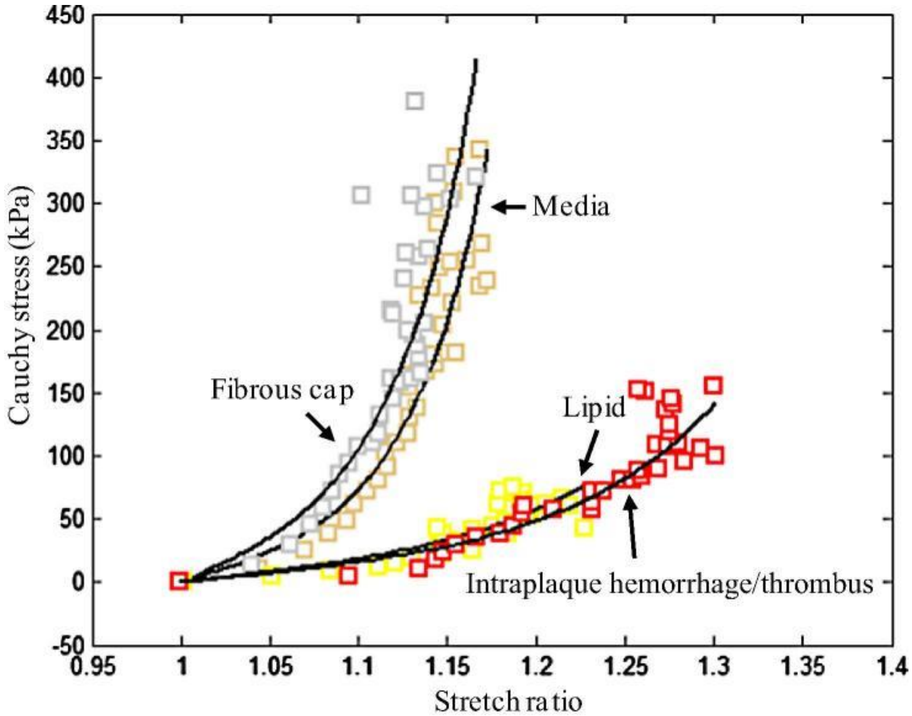

Figure 13. Cauchy stress-stretch ratio of different plaque components [22]

The behavior of the plaque is also shown on Figure 13 from a research on the material properties in human carotid atherosclerotic plaques. In addition to properties discussed previously, a compiled study of the human carotid plaques is also shown on Figure 14.

Studies of direct material measurements on human carotid atherosclerotic plaques.

Author	Samples (n)	Method	Tissue type	Main conclusions
Learoyd and Taylor	7	Expansion	Whole plaque	Incremental Young's modulus at internal pressure of 40 mmHg was about 250 kPa, at 110 mmHg was 1000 kPa and at 160 mmHg was 3000 kPa
Ebenstein et al.	10	Nano-indentation	Hematoma and fibrous tissue	Young's modulus of hematoma was 230 ± 210 kPa and the one of fibrous tissue was 270 ± 150 kPa
Teng et al.	6	Uniaxial extension	Intima thickness with/without small lipid	The material strength of adventitia was 1996 ± 867 kPa and 1802 ± 703 kPa in the axial and circumferential directions respectively and the corresponding value of media was 519 ± 270 kPa and 1230 ± 533 kPa. Adventitia, media and intact specimens exhibited similar extensibility at failure
Maher et al.	14	Indentation and uniaxial extension	Not mentioned	Calcified plaques had the stiffest response, while echolucent plaques were the least stiff
Barrett et al.	8	Indentation	FC	The inferred shear modulus was found to be in the range 7–100 kPa with a median value of 11 kPa
Lawlor et al.	14	Uniaxial extension	Whole plaque	Experimental Green strains at rupture varied from 0.299 to 0.588 and the Cauchy stress observed in the experiments was between 131 and 779 kPa
Kural et al.	5	Biaxial test	Not mentioned	The Young's modulus was 0.91–4.64 kPa in longitudinal direction and 1.32–6.38 kPa in circumferential direction
Chai et al.	8	Indentation	FC and lipid	Young's modulus of fibrous tissue was found in the range from 6 to 891 kPa (median 30 kPa) and the one of lipid ranged from 9 to 143 kPa (median 16 kPa)
Mulvihill et al.	25	Uniaxial extension	Whole plaque	Rupture stress value for the lipid-dominated plaques is 342 ± 160 kPa and the value for stiffer plaques (calcium to lipid ratio >1) is 618 ± 230 kPa
This study	21	Uniaxial extension	FC, media, lipid and intraplaque hemorrhage/thrombus (IPH/T)	The stiffness of FC and media was comparable and so was lipid and IPH/T. Both FC and media were much stiffer than either lipid or IPH/T

Figure 14. Different studies on material properties of human carotid atherosclerotic plaques [22]

Based from the different studies mentioned previously, arteries and plaque are generally anisotropic and heterogeneous in nature which may incur variations in different areas. It may therefore still be necessary to infer knowledge and experience from cardiac surgeons and related professions for evaluating the realism of the printed phantoms despite the multitude of studies regarding the mechanical properties.

3. Plaque (disease) locations

It has been identified that 20% of coronary intervention treatments have been at the coronary bifurcation lesions and 50% of occurs at left-main artery bifurcation lesions. [23]. Characterizations have been therefore developed to classify different types of disease development in different sections of the coronary bifurcation. The Medina classification is a simple and often used method to classify this and is shown on Figure 15. ("1") indicates a presence of stenosis while ("0") indicates its absence from either the main branch proximal lesion, main branch distal lesion or side branch lesion. An imaging process such as ultrasound is necessary in order to detect these in a patient.

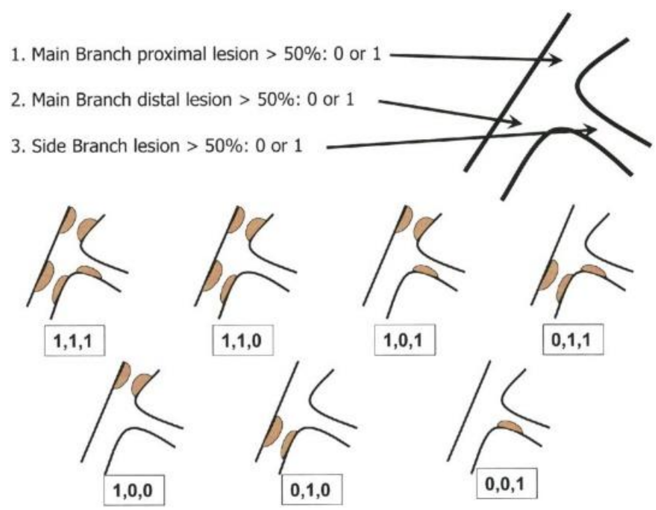

Figure 15. Medina classifications for bifurcation lesions [23]

The statistic regarding the occurrence of each medina classification however is yet to be identified and will require additional research. A study regarding the effect of the bifurcation angle however has shown that there is a significant correlation with the presence of lipid arcs [24].

4. Research Question and Project Plan

While there have been multiple studies on the hemodynamic analysis of blood flow in the coronary artery, based on the previous section there is a lack of studies that has touched upon the use of more accurate representation of the mechanical properties of the coronary artery walls and the plaque disease. This research will aim to replicate and evaluate the relevant mechanical properties of the coronary artery with the use of available 3D printing resources in UNSW and establish a method to produce the phantom replica.

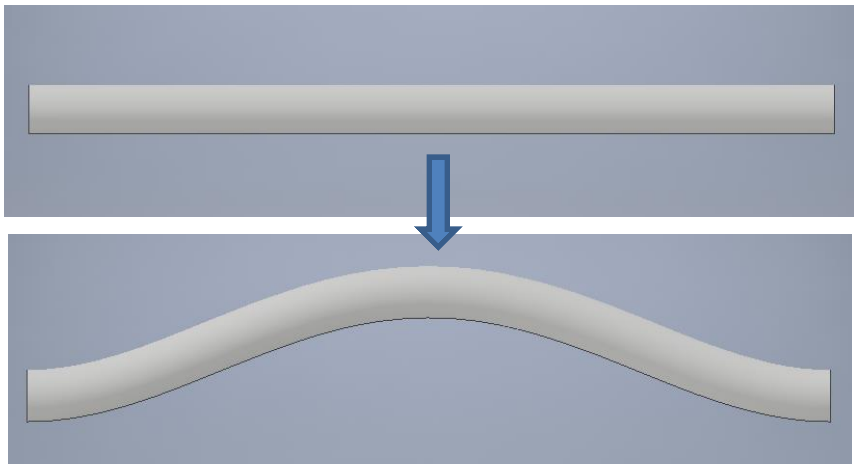

Figure 16. Changing the shape to a sinusoid

In theory, in order to change a certain material's stress-strain curve to a more convex shape or any other shape, the material's shape or design must be changed such as shown on the image above. The effect of this change to a sinusoid as seen in the figure below is similar to how human tissue behaves.

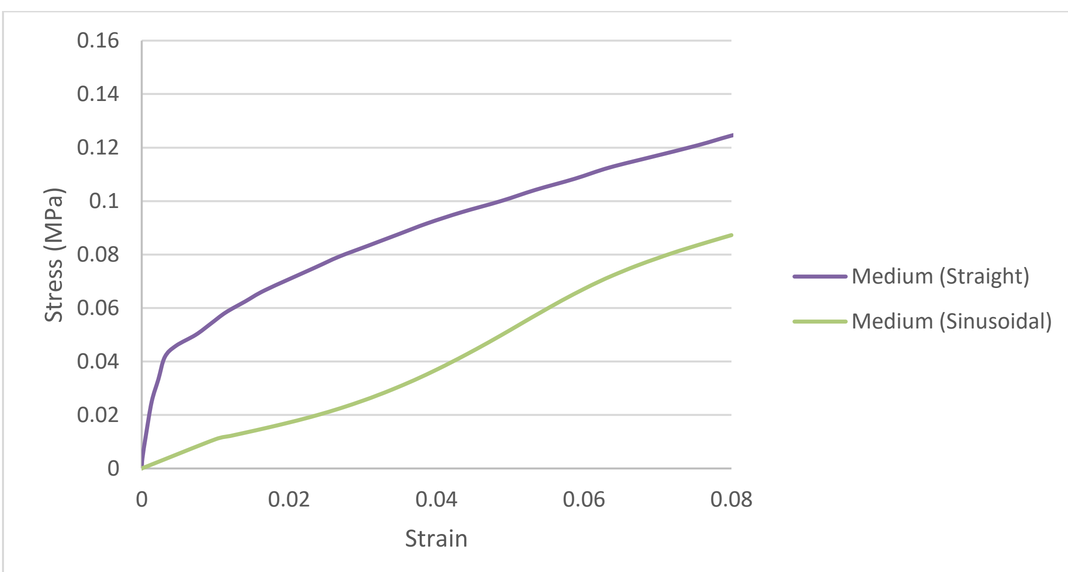

Figure 17. Effect of changing the structure shape on the stress-strain curve

A blood vessel is however not just a single strand of fibre aand will therefore need to be combined with a matrix and the effect of the matrix will be further explained in the following sections of the report.

Some of the potential benefits of this research may be the following:

- Comparisons with commonly used materials for phantoms and more accurate representations of the mechanical properties of the arteries may be evaluated.
- Multiple models for different disease stages and populations may be developed for future studies and applications.
- A method for producing more accurate 3D printed arterial phantoms may serve as basis for further personalized cardiovascular studies to improve clinical practice.
- Evaluating the effects of vessel wall elasticity, shape and flow at the cellular level may be applied for future studies.

Several 3D geometries will be created in order to properly evaluate the mechanical properties and behaviour in of the material used from the 3D printer. The main study will be focused on the left main bifurcation that divides the left anterior descending (LAD) and circumflex (LCX) arteries. The different geometries to be evaluated are the following:

- 3D geometry with dimension based on ASTM D638
- Coronary Artery 3D representations (with and without disease)
    - Simplified geometry of an artery with bifurcations
    - 3D geometry scanned from a real coronary artery
    - Meta-material structures

While these are the different geometries to be attempted, other factors and details such as different materials representing different arterial layers will also be observed.

a. Timeline

The time and duration of training, testing and evaluations are shown in the Gantt Chart (Appendix A). The main evaluations to be conducted are detailed as follows:

- 3D Geometry creation for test print
- 3D Printer multi-material test print
- 3D Geometry creation for evaluation of properties based on different 3D printer parameters
    - Testing according to ASTM D638 to attain the mechanical properties which is similar to the test method used for 3D system's raw materials.
- 3D Geometry creation for evaluation of properties based on different materials

- Testing according to ASTM D638 to attain mechanical properties.
- Property comparisons with other experiments from related literature.

b. Resources required:

- 3D Printer
- 3D Printer materials

c. Training and skills obtained:

- Software
    - Autodesk Meshmixer
    - Computer Aided Design Software: Solidworks / Autodesk Inventor
    - 3D Printer software
    - ANSYS
- Hardware
    - 3D Printer machine operation training
    - Tensile testing equipment training

Figure 18. Tensile Test Machine

III. Methodology

1. 3D Geometry preparation

a. Initial Prints

As an initial test geometry to print on the 3D printer, a coronary artery with a plaque representing disease is generated using Autodesk Meshmixer 3.5 and Solidworks 2017. The coronary artery internal surface geometry is from a scanned patient coronary artery at the left main coronary artery bifurcation. This surface geometry is then converted into a solid with an initially applied 1mm thickness using Autodesk Meshmixer. The plaque geometry is then applied in the solid geometry using Solidworks.

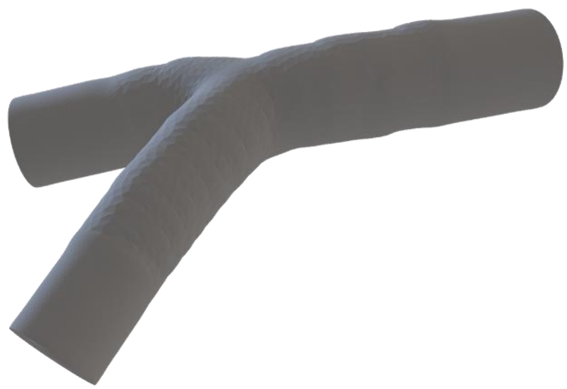

Figure 19. 3D Geometry of coronary artery

Additional 3D geometry for different Medina Classifications will be made depending on the related research. For the first geometry a (1,0,0) classification is created for initial testing on the 3D printer.

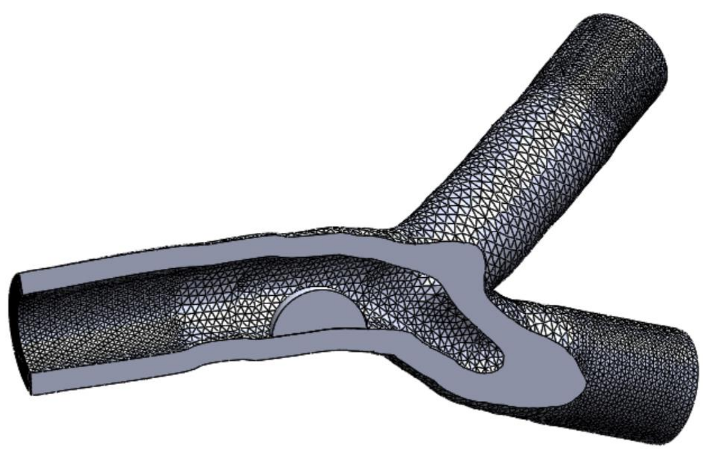

Figure 20. Section Cut showing 3D geometry generated plaque

A simplified model of the coronary is modelled as shown on the figure below. The model is a simplified bifurcation with 2 small circular bodies that represents the plaque or disease. Using Autodesk Inventor, the

2 plaque bodies are made separately from the main vessel body in order for the 3D printer software to recognize that the bodies are separate entities. The plaque body is made big enough to represent around a 50% stenting and enough to have a little bit of protrusion outside of the vessel wall's body.

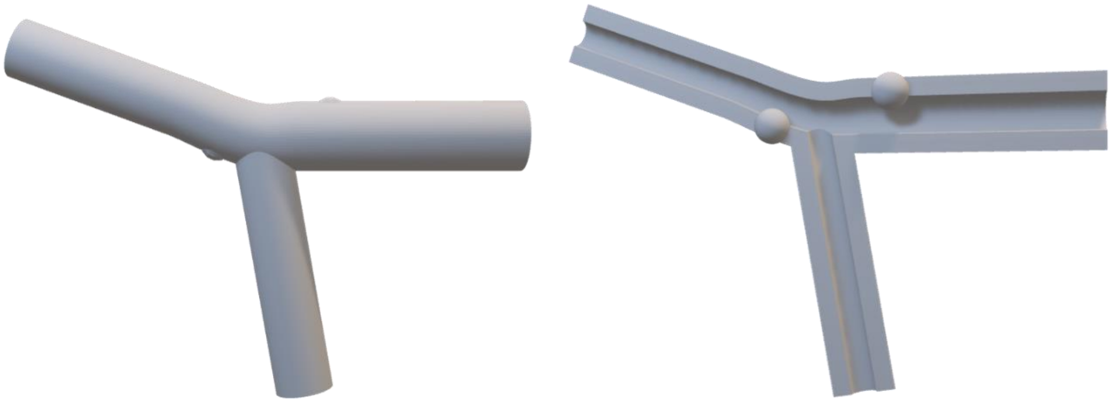

Figure 21. Full and Half body of the simplified bifurcation geometry

b. Meta-material structure

As shown in Figure 22, an arterial blood vessel wall's structure is commonly described with a three-layer architecture: the intima, media and adventitia. These layers are composed of an extracellular matrix (ECM) comprised of a complex meshwork of different cell fibres and molecules that provides the vessel its mechanical properties. [25]

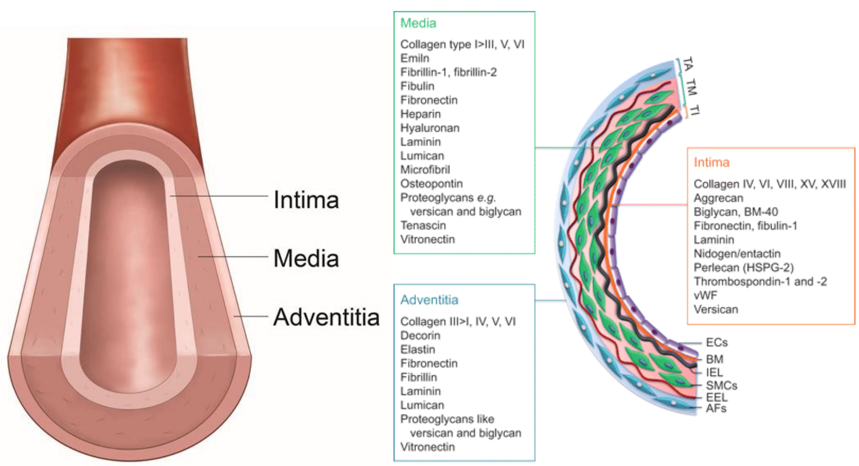

Figure 22. Arterial vessel wall three-layer architecture and its extracellular matrix (ECM) components [25]

In order to mimic the vessel's properties, a metamaterial structure is to be modelled. To determine the necessary shape, dimensions and materials to use for the metamaterial structure, a simple model as shown on the right of Figure 22Figure 23 is initially made for simulations. This geometry is similar to the model studied by Wang et al. wherein a sinusoidal wave element represents the dominant fibres found in the ECM (such as collagen) that will ideally cause the metamaterial behave similar to soft tissue.

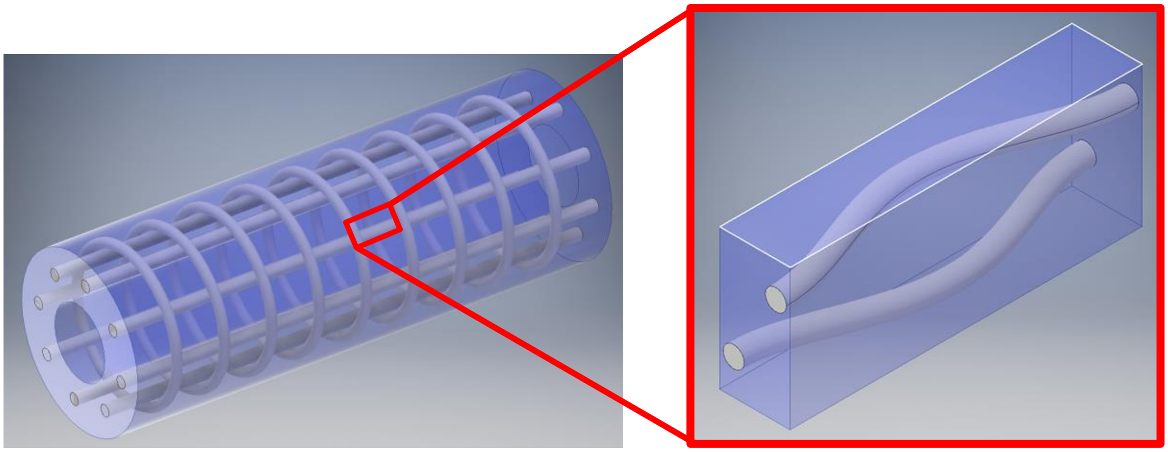

Figure 23. Simple metamaterial structure for a blood vessel (left image: Simplified representation of a complete structure for a blood vessel wall layer. Right image: Actual representation of a section of the overall structure for initial simulations and experimental testing)

The image on the right of Figure 23 is the initial shape to be used for the simulation. The structure contains two parts; the matrix (blue transparent block) and the fibres (2 grey sinusoidal shapes). In theory the initial strain of the metamaterial will follow a curve similar to the matrix material until the curve starts to follow the fibre material's curve once the wave straightens as the whole structure is stretched [26]. The 2 sinusoidal fibres are modeled with only 1 wavelength long (10mm), an amplitude of 0.6mm and fibre radius of 0.3mm. The cross sectional dimension of the matrix block is 4mm by 2mm while the block length is equivalent to the fibre wavelength.

2. *3D Printing*

The 3D printer identified to be used for this research is the newly installed Projet MJP 5600 3D printer from 3D systems. This is located in J18 Willis Annexe at UNSW. This printer is a multi-material 3D printer that can print using a combination of different 3D system's multijet materials. These materials can be either rigid or elastomeric as well as either black, white or translucent. [12] In addition to support materials, the two materials specifically identified to be used and purchased initially are the following:

- VisiJet CR-CL 200 (Rigid) – cost: $862 for one 2.0kg bottle
- VisiJet CE-NT (Elastomeric) – cost: $862 for one 2.0kg bottle

Figure 24. Projet MJP 5600 [12]

An initial training was provided by 3D systems to UNSW that explained how to properly use the printer. During this training session, some of the few key points are:

- there is a software manual that can be accessed online
- a free version of the software may also be accessed
- can use software to change materials to part but will need the part to be either as assembly file converted to stl. However, when doing an initial test, the method wasn't working well so there may be a need to use multiple stl files and combine them into one structure using the 3d printer software
- density cannot be directly changed apart from just using different materials and/or combination of material
- the machine can print to as small as 13micrometer thickness

The table below shows the materials used for the printed part. Four parts were initially printed using different materials for comparison with each other. The materials selected were based on the properties found in Figure 25.

Table 1. Material Assignment for initial samples printed

Part Sample	**1**	**2**	**3**	**4**
Vessel Body	A80	A60	A80	A90
Disease Body 1	D70	CL	CL	CL
Disease Body 2	A50	NT	NT	NT

All four of the samples from Table 1 were printed using just the half body of the simplified model. Judging from the materials printed, all the vessel bodies printed (A60-A90) based on just touching the material felt too stiff comparing it to what an actual vessel body might be, while the CL and NT materials were easily distinguishable as the CL material is the stiffest material while NT was the softest material.

After realizing the stiffness of the materials from A60-A90, additional prints were made using A50 instead for the vessel's body, and CL and NT for the two disease bodies. One sample was made using the half body geometry and one sample was made for the full body geometry as well. This resulted in a softer vessel body which seems to be closer to the actual coronary vessel. This may however by more accurately judged by a future evaluation made with the aid of expert clinicians such as heart surgeons.

Properties	Condition	VisiJet CR-BK	VisiJet CR-WT 200*	VisiJet CR-CL 200*	VisiJet CE-NT	VisiJet CE-BK
Composition		UV curable plastic	UV curable plastic	UV curable plastic	UV curable elastomeric	UV curable elastomeric
Description		Rigid ABS-like	Rigid ABS-like	Rigid polycarbonate-like	Elastomeric	Elastomeric
Color		Opaque black	Opaque white	Translucent clear	Translucent natural	Opaque black
Bottle Quantity (kg)		2	2	2	2	2
Solid Density (g/cm^3)		1.16	1.16	1.16	1.12	1.12
Tensile Strength (MPa)	ASTM D638	37-48	33-40	30-43	0.2-0.4	0.2-0.4
Tensile Modulus (MPa)	ASTM D638	1800-2500	1500-2000	1400-2100	0.27-0.43	0.27-0.43
Elongation at Break	ASTM D638	5-11 %	12-22 %	14-22 %	160-230 %	160-230 %
Flexural Strength (MPa)	ASTM D790	67-80	47-52	40-60	N/A	N/A
Flexural Modulus (MPa)	ASTM D790	1800-2300	1200-1700	1100-2000	N/A	N/A
Impact Strength (Notched Izod) (J/m)	ASTM D256	17-24	21-24	21-30	N/A	N/A
Shore A Hardness	ASTM 2240	N/A	N/A	N/A	27-33	27-33
Shore D Hardness	ASTM 2240	78-83	77-80	77-80	N/A	N/A
24 hr Water Absorption	ASTM D570	0.5%	0.5%	0.5%	0.9%	0.6%
Heat Distortion Temp @ 0.45 MPa @ 1.82 MPa	D648	54-61 °C 48-49 °C	42-47 °C 40-44°C	42-50 °C 40-44°C	N/A N/A	N/A N/A
Tear Resistance (kN/m)	ASTM D624	N/A	N/A	N/A	3.1 - 3.7	3.1 - 3.7

PROPERTIES	ASTM	MULTI-MATERIAL COMPOSITES (VisiJet CR-CL 200** + VisiJet CE-NT)										
Material Name		RCL-ENT-D75	RCL-ENT-D70	RCL-ENT-D65	RCL-ENT-D60	RCL-ENT-D55	RCL-ENT-A90	RCL-ENT-A80	RCL-ENT-A70	RCL-ENT-A60	RCL-ENT-A50	RCL-ENT-A40
Description		Very rigid	Slightly rigid	Rigid	Rigid	Slightly rigid	Slightly flexible	Slightly flexible	Flexible	Flexible	More flexible	Very flexible
Appearance*		Very clear white	Light clear white	Light clear white	Light clear tan	Light clear tan	Medium clear tan	Medium clear tan	Medium clear tan	Translucent tan	Translucent amber	Translucent amber
Tensile Strength (MPa)	D638	19-27	12-16	8-10	4-5	2-3	1.4-1.9	1.3-1.7	.75-1.1	.48-.77	.35-.48	.23-.32
Flexural Strength (MPa)	D790	18-21	12-13	7-7.4	3.9-4.2	1.6-1.9	N/A	N/A	N/A	N/A	N/A	N/A
Flexural Modulus (MPa)	D790	450-750	350-550	150-250	70-180	30-80	N/A	N/A	N/A	N/A	N/A	N/A
Impact Strength (J/m) (Notched Izod)	D256	18-25	22-30	32-52	29-42	74-114	N/A	N/A	N/A	N/A	N/A	N/A
Shore A Hardness, Scale A	D2240	N/A	N/A	N/A	N/A	N/A	86-92	75-85	65-75	55-65	45-55	35-45
Shore D Hardness, Scale D	D2240	70-80	65-75	60-70	55-65	50-60	N/A	N/A	N/A	N/A	N/A	N/A
Tear Resistance (kN/m)	D624	N/A	N/A	N/A	N/A	N/A	44-62	25-32	18-23	11-17	6.6-9.3	6.5-8.5

*Visual approximation. No guarantee that part output will match exactly to software or datasheet values.
** Respectively replaces former VisiJet® CR-WT and VisiJet® CR-CL

Figure 25. ProJet MJP 5600 3D Printer Material List [12]

3. Material Tensile Testing

In addition to the simplified geometry prints, tensile test specimens were then printed using A50, NT and CL as well. These were made in order to determine mechanical properties particularly the stress-strain curves of the material which were not initially provided by the 3D printer material supplier.

The specimen dimensions shown on Figure 27 are based on a Type IV specimen from the ASTM Standard D638-14 which is the standard test method for tensile properties of plastics. The parts are printed on a horizontal orientation as shown in Figure 26. This part orientation was initially chosen to reduce printing time. The part printed at a horizontal orientation has an estimated completion time of just 3 hours compared to the vertical orientation which is 30 hours of estimated printing time. This is due to the method of material jetting 3D printers wherein the time needed for UV light to cure each layer before proceeding to the next is the same for each layer despite printing the same volume.

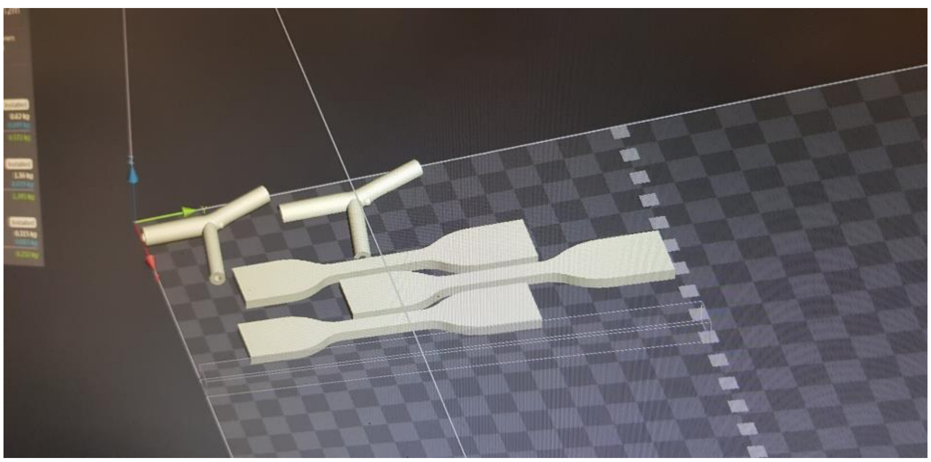

Figure 26. Screen capture from the 3D printer software of the Tensile specimens and the Full and Half body simplified vessel geometry using A50, NT and CL materials

In a study made by JRC Dizon et al. on mechanical characterization of 3D-printed polymers, it was mentioned that part orientation has some significance in the stiffness of a polyjet printed material but has less on an effect on the ultimate stress [27]. While only the prints shown above were initially completed, prints for vertical orientation are also to be completed in the future in order to determine the difference in mechanical properties compared with vertical and horizontally oriented parts. To continue with the study however, it is assumed that there are minimal differences from the horizontal and vertical orientations from parts printed using material jetting printers such as the MJP 5600.

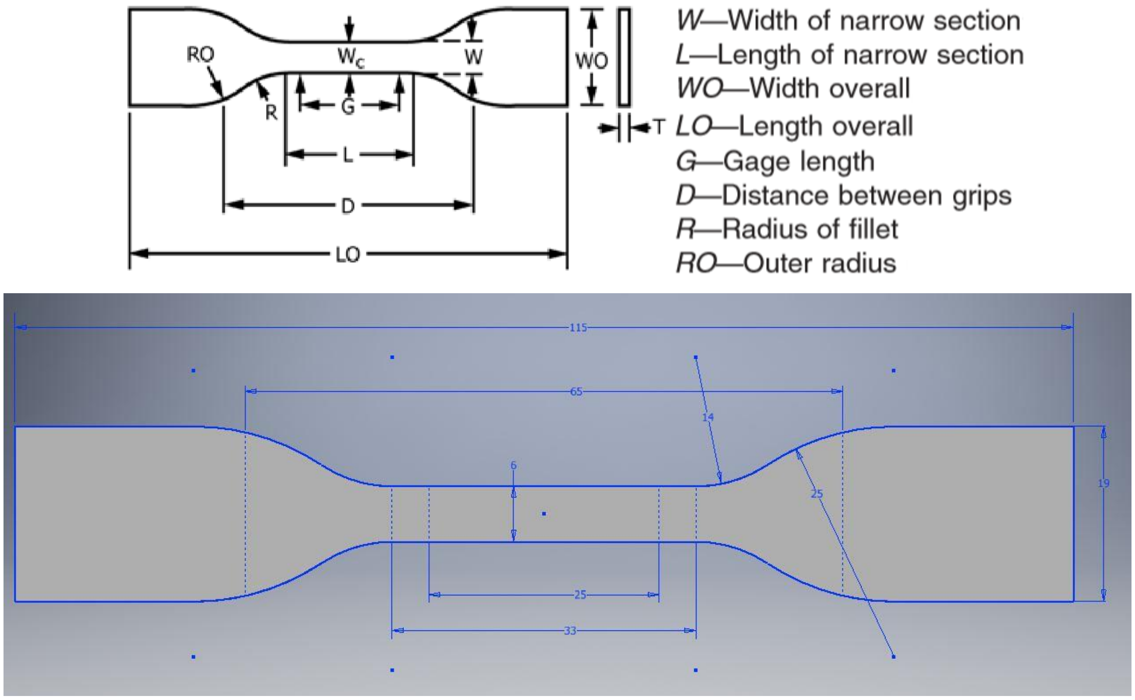

Figure 27. Tensile Test Specimen dimensions based from ASTM Standard D638-14 [28]

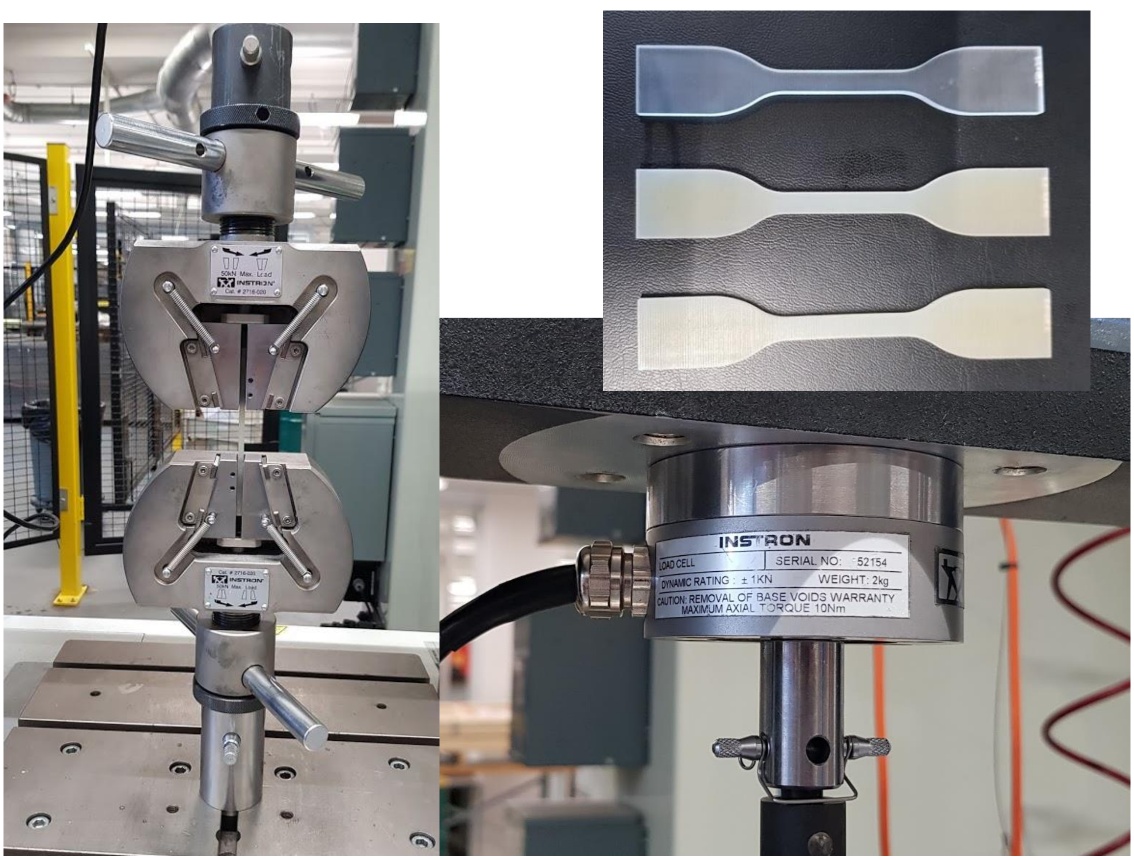

Figure 28. Tensile Test set-up

Following the procedures from the ASTM Standard, the tensile test was performed with a testing speed of 5mm/min for the stiff material (CL) and 50mm/min for the flexible materials (A50 and NT). The test was conducted using the INSTRON 3369 in Willis Annex Building of UNSW Sydney. The smallest load cell available of 1kN was deemed suitable for this application as the smaller load cell can give more precise measurements than its larger counterparts. This is especially important for this application since most of the properties to be analyzed are in the strain region of about 5% which is wherein the pressure from a human cardiac cycle undergoes large deformations *in vivo* [29] [30] [31]. The strain region may still vary from each patient and there is a possibility of reaching strains of upto 25% depending on the situation [26].

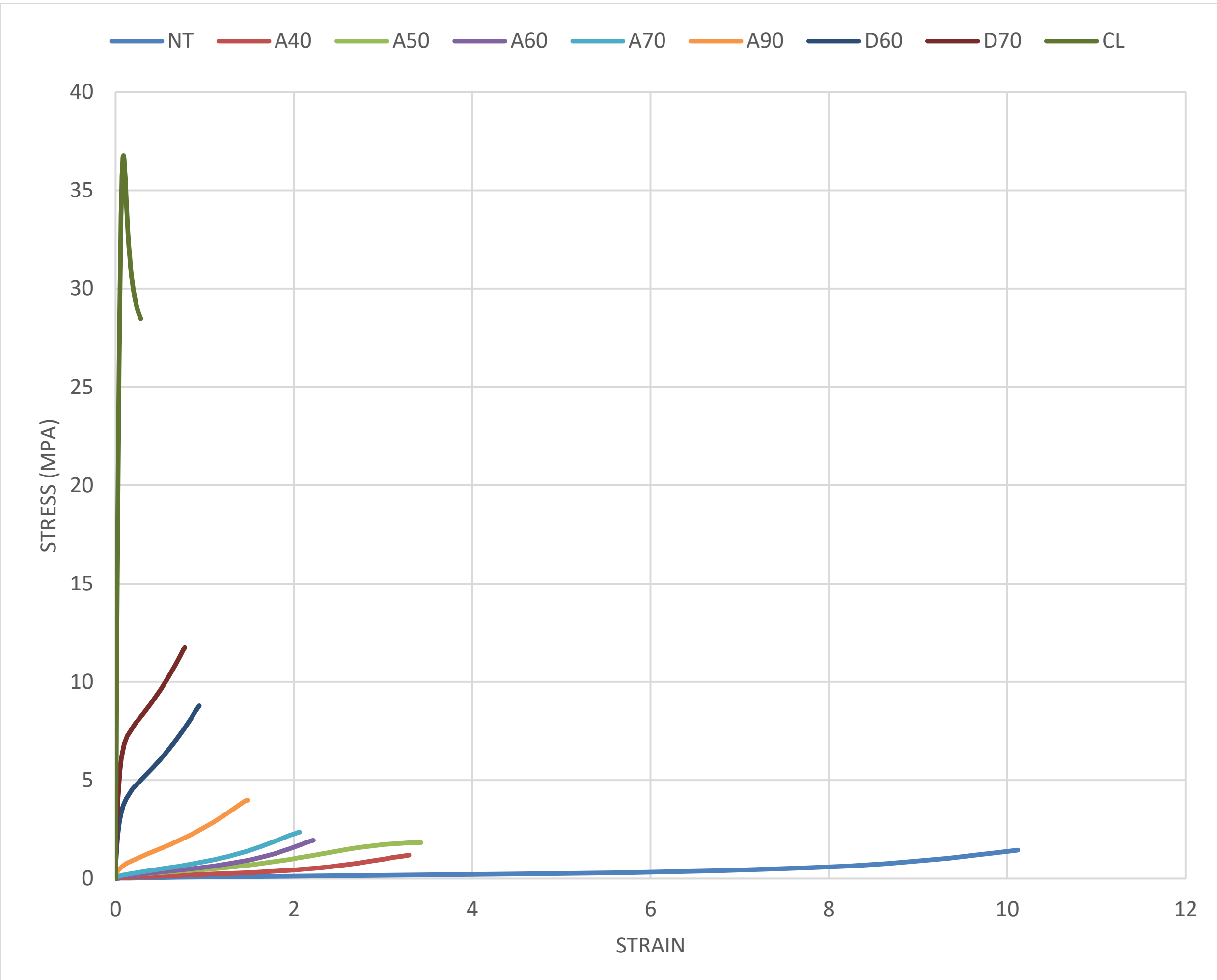

Figure 29. Stress – Strain data for other 3D printer materials.

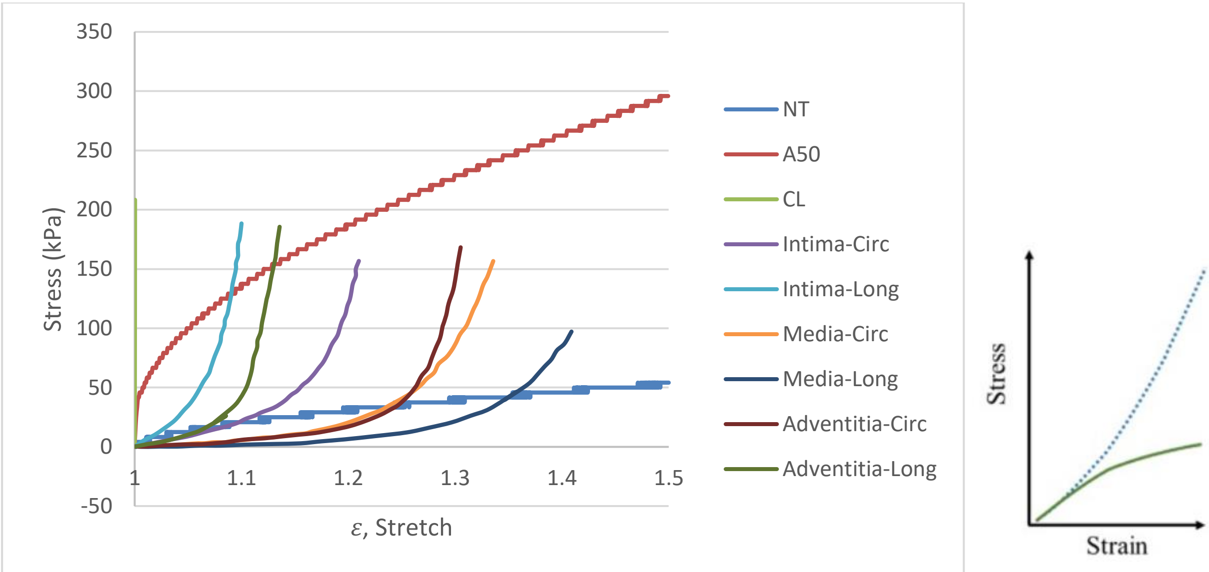

Figure 30. Stress-strain curve comparison of the 3D printed polymers and the blood vessel tissues side by side with related literature. [15] [26]

For the purpose of this study, the hardest material (CL) and softest material (NT) shall be referred to as Hard and Soft respectively, while any combination of the two will be referred to as Medium. The preliminary simulations is shown in the table below.

Table 2. Materials for Preliminary Simulations

Material Description	**Soft**	**Medium**	**Hard**
Material Name	VisiJet CE-NT	RCL-ENT-A50	VisiJet CR-CL 200
Stress-Strain Curve	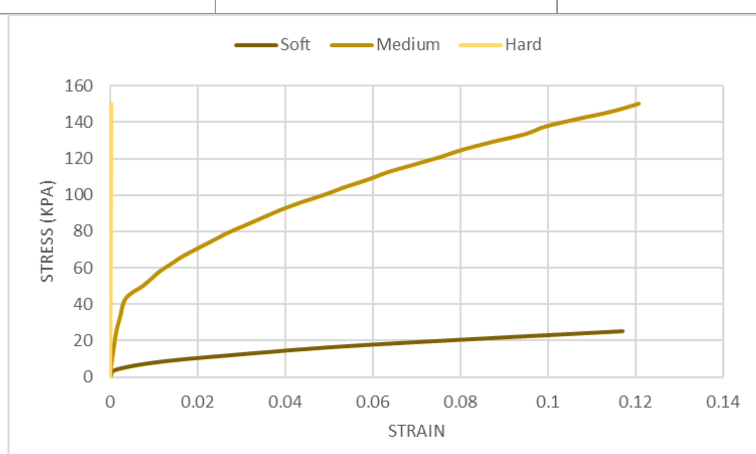		

The tensile test results for each of the materials are shown above. As expected from a stiff material, CL is shown to have a very steep stiffness curve (Young’s Modulus>500 MPa) while the other two materials

(A50 and NT) show a lower curve concaving with the A50 and NT having stress values approximately 140kPa and 25kPa respectively at 10% strain.

Comparing the stress-strain curve of the printed materials and the tissues, it resembles the study made by Wang et al, regarding the use of metamaterials to mimic the behavior of soft tissues as the curve for tissue go upward while the polymers concave down. It also shows that NT material, may be used as the main matrix material for an arterial vessel as it is the closest match to the behavior of the tissue at its initial creep. A limitation however is that a softer or more flexible material that NT will be required if certain tissue types such as the media tissue are to be mimicked as there currently no available or existing materials softer than NT for this 3D printer.

4. Computer Simulation

The model is imported into ANSYS from Autodesk inventor using a saved (.stp) file to be used in a static structural analysis system. The material curve data as shown in Appendix A taken from tensile tests are defined in ANSYS using a multilinear kinematic hardening model as the curves were nonlinear. The mesh resolution was set to 2 for quicker simulations as a validation study detailed in Appendix B shows that there are is negligible difference in the results with a higher mesh resolution setting. Large deformation setting is turned on with 8 substeps for a more defined resulting curve. One end of the model was fixed in all directions while the other end is set with a displacement to match strains of upto 8%.

IV. Results and discussion

1. Preliminary Results

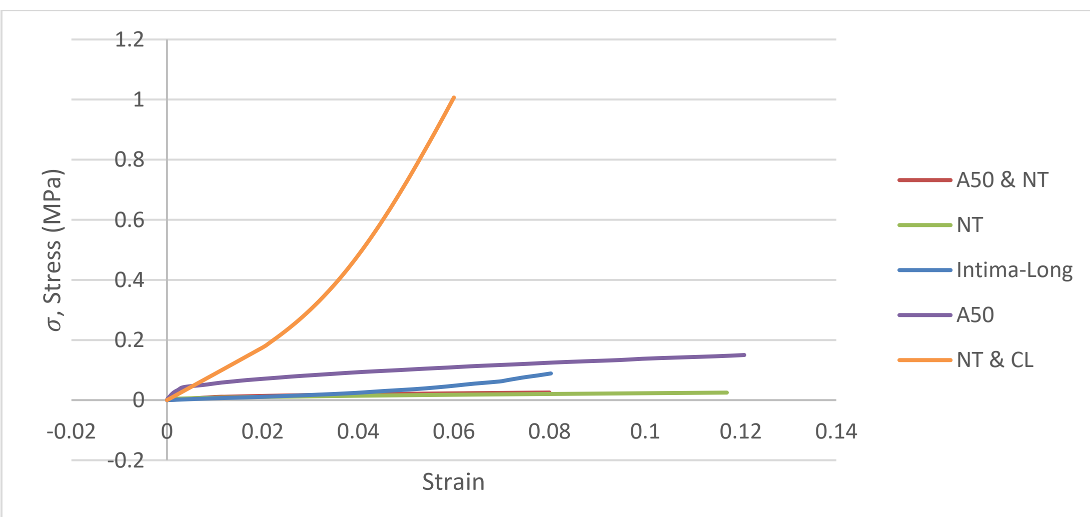

Figure 31. Curve comparison if the material used for the wave element is A50 vs CL

The results for both the medium(A50) material and hard(CL) being used for the wave element are shown above. It can be observed that while resulting curve of soft(NT) & CL resembles the upward curving shape of soft tissues, there is a big gap between the property of the soft tissue being compared (in this case is the intima stretched at a longitudinal direction). The result of using A50 & NT shows a curve that is closer to the soft tissue but does not resemble the same curve shape as seen more clearly from the figure below.

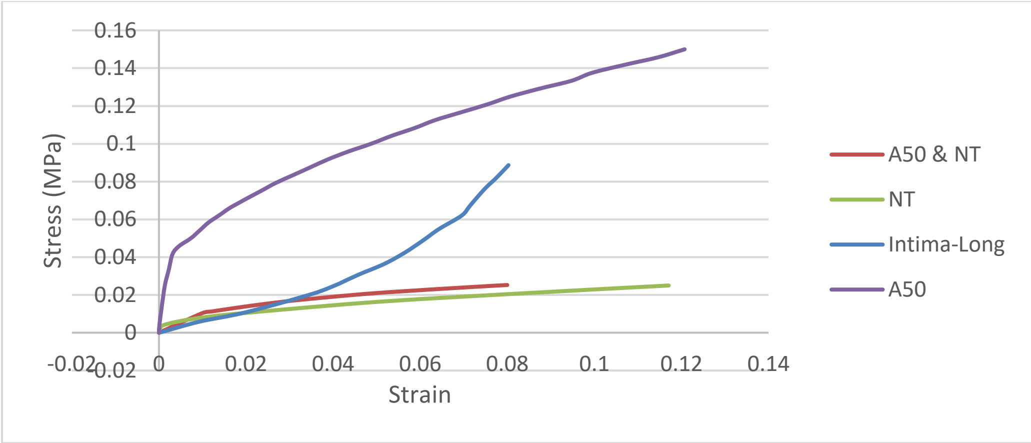

Figure 32. Curve comparison of wave element using A50 with longitudinal Intima properties from related literature.

Other shapes and other parameters regarding the structure of the metamaterial may be changed as well such as the sinusoidal wave amplitude, wavelength and radius. For Figure 33, the amplitude of the wave is changed from 0.6 to 0.3. In this case, there was not much difference in the result however for further studies, other shapes and parameters will then be applied more for better comparisons since the parameters set for this material may not be effectively displayed due to the little difference between the properties of the medium (A50) and the soft material.

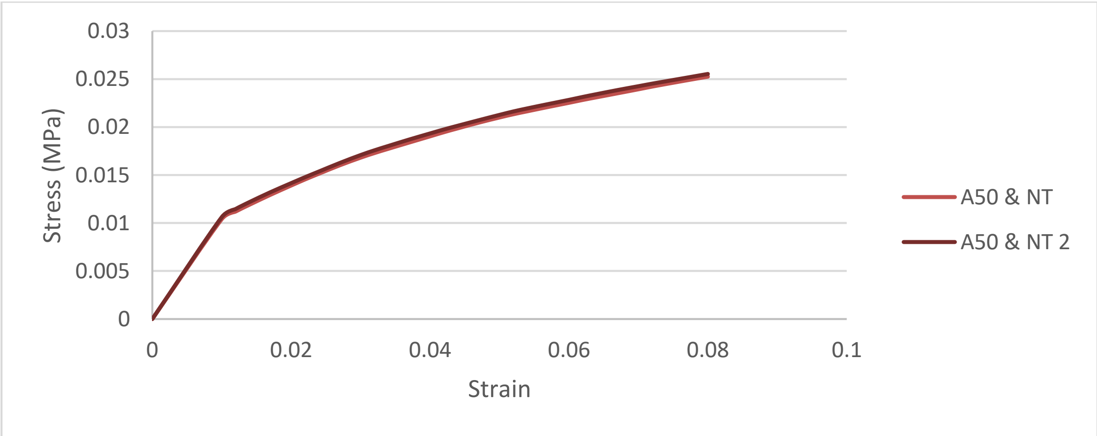

Figure 33. Curve comparison of changing the amplitude of the wave element

a. Summary of Preliminary Results

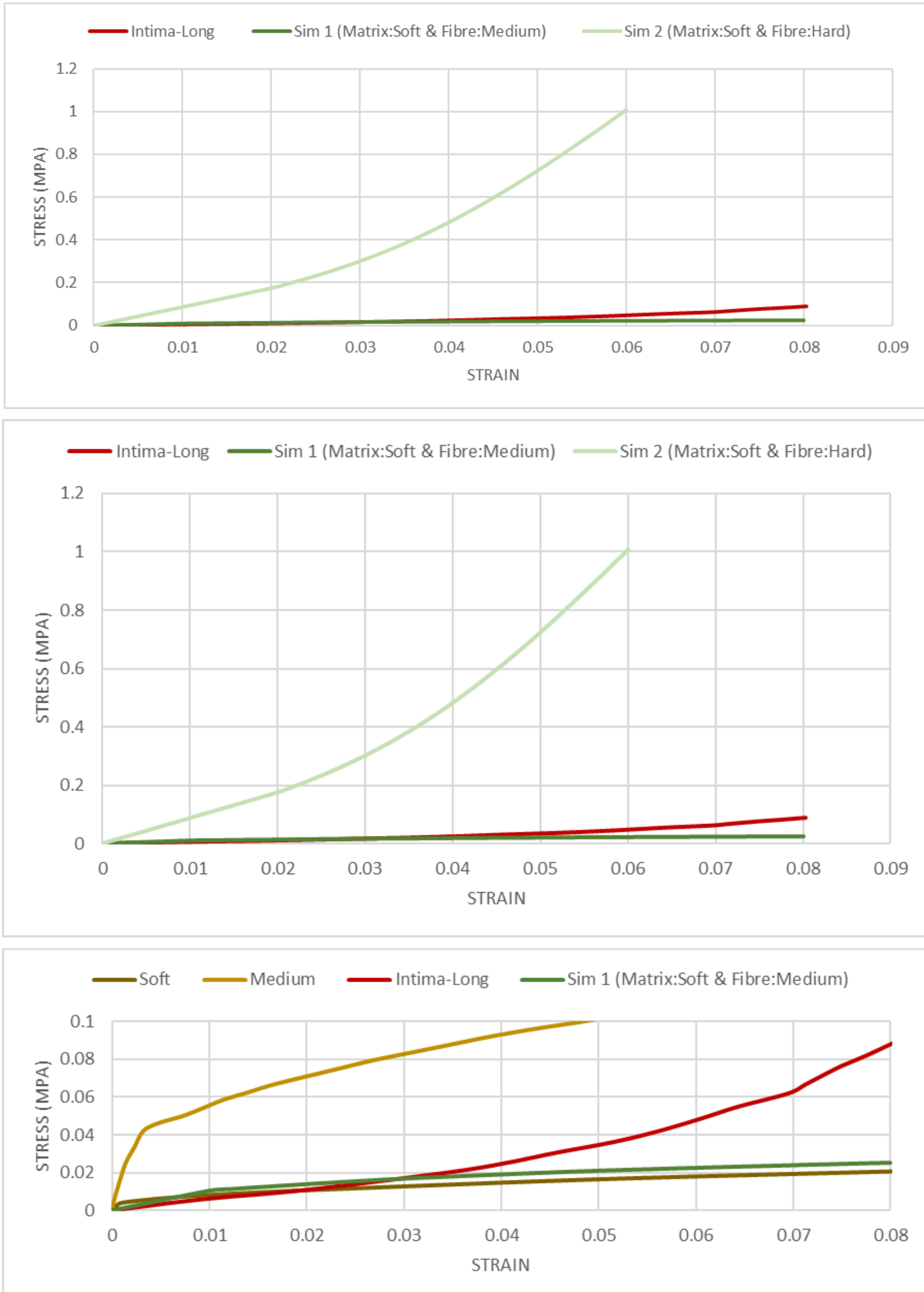

Figure 34. Stress-strain curve summary for preliminary results

It can be observed that the resulting curve of Sim 1 is similar to the intima curve and the soft (matrix) material curve at the initial strain of up to around 0.04. Then the intima curve starts to separate from the Sim 1 curve as the intima starts to have a steeper slope while the Sim 1 curve maintains almost the same curve shape as the soft material. This indicates that the fibre material's parameters for Sim 1 does not significantly change the metamaterial's curve from the matrix material curve.

As for Sim 2, it behaves similarly with the intima as both curves get steeper slopes as the strains increase, however, the stress results of Sim 2 are much higher maybe due to the significantly stiffer fibre material used. This nevertheless indicates that the addition of the fibre shape to the matrix can result to am upward curve shape similar to soft tissues and that the shape of the fibre may still have an influence on the curve's characteristics such as the slopes at the initial strain and the point of which the curve starts to increase in steepness.

Additional simulations are performed to determine the effects of the following fibre parameters: amplitude (A), wavelength (λ), radius (r), and material.

2. Simulation Validation and Verification

a. Simplified model verification

To verify wether the simplified model can accurately reflect an application similar to what an actual blood vessel may look like, a cylindrical model is made for comparison.

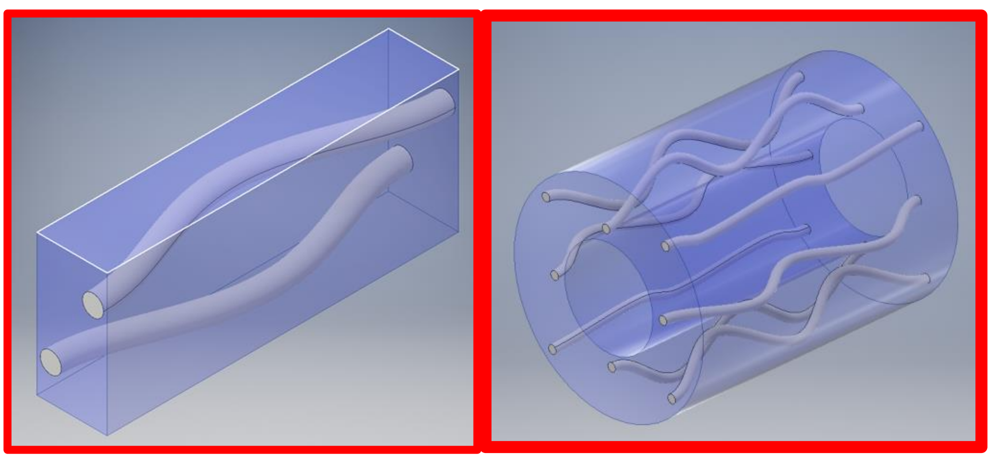

Figure 35. Simplified model(Rectangular) vs Blood vessel model(Cylindrical)

Results verify that the simplified model can be used for further simulations as there is minimal difference between the mechanical behaviour of the two models as shown in Figure 36.

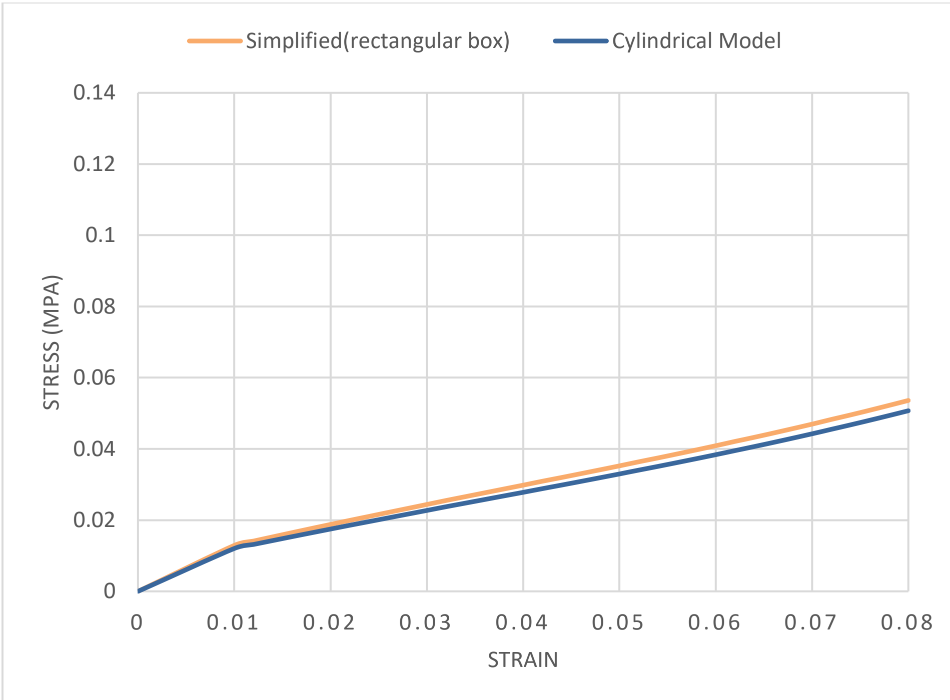

Figure 36. Simplified model(Rectangular) vs Blood vessel model(Cylindrical) Stress-Strain curve

b. Comparison with related literature

In order to validate the simulations from ANSYS, the metamaterial simulation of the sinusoidal wave was compared with the results from the related literature. Using the same material used from article, the material curves shown below were put into ANSYS and applied to the same geometry used from the study by Wang et al.

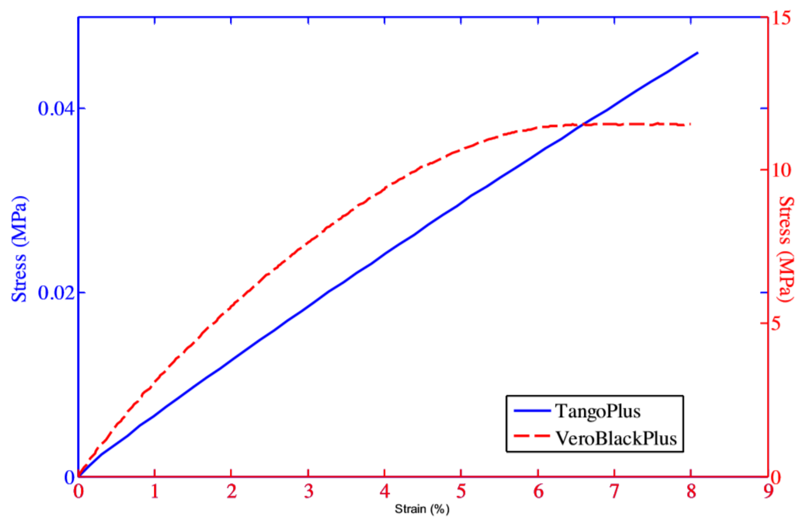

Figure 37. Material used from reference article [32]

The stress contour as shown from the figures below show similar areas of high and low stresses. The main difference was that the result of the new simulation was lower by about 1MPa. The curve shown in Table 3 and Figure 38 shows that the new simulation had a lower stress result as well by around 0.1(MPa) less.

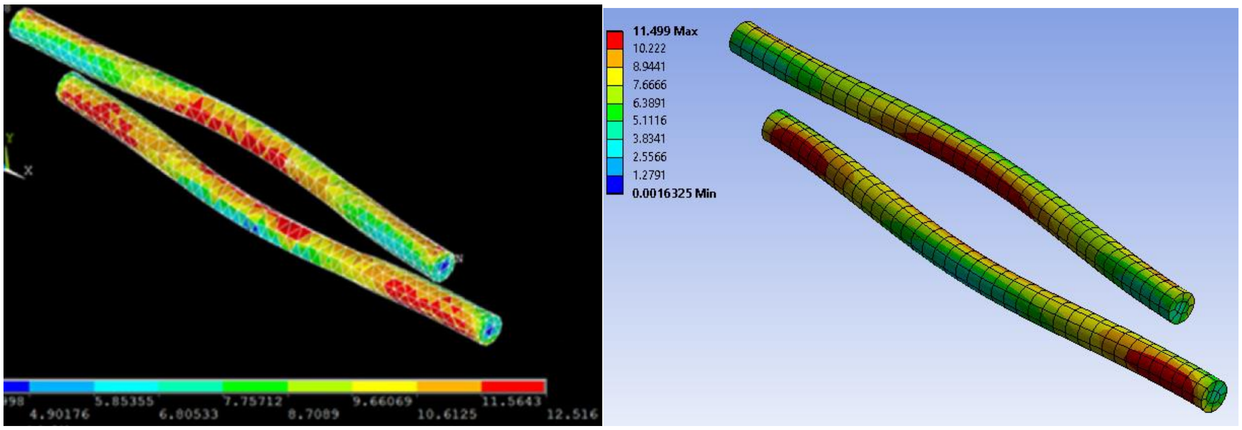

Figure 38. Comparison of Stress contour for the wave elements from literature(left) [32] and new simulation(right)

This difference may be due to the difference in mesh. There is therefore a need to possibly improve the mesh. Some errors may also be present during the material input since the data points taken from the material curve may have some slight discrepancies to the original data points due to it being taken manually using a web plot digitizer software. In order to further validate the simulation, a sample 3D printed part may also be tested.

Table 3. Simulation Validation and Mesh Verification

Simulation	Unrefined mesh	Refined mesh
Mesh Resolution	2	6
Nodes	11581	49089
Elements	2102	23613
Simulation Time	15min	1hr 20min
Matrix Mesh Image	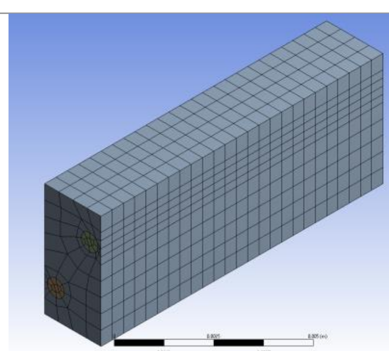	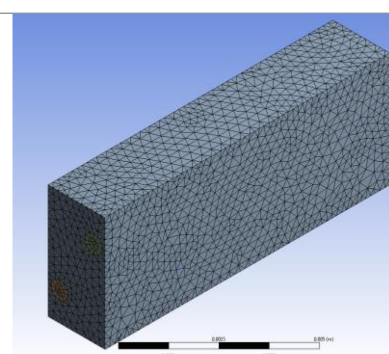

<table>
<tr>
<td>Fibre Mesh and Deformation</td>
<td>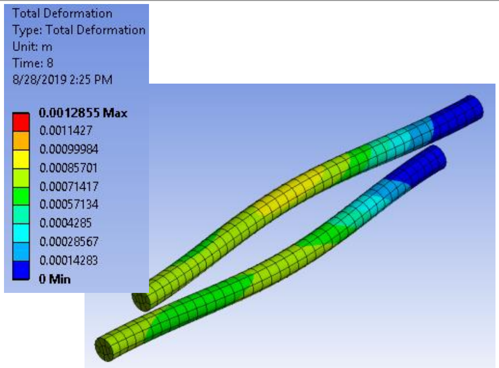
</td>
<td>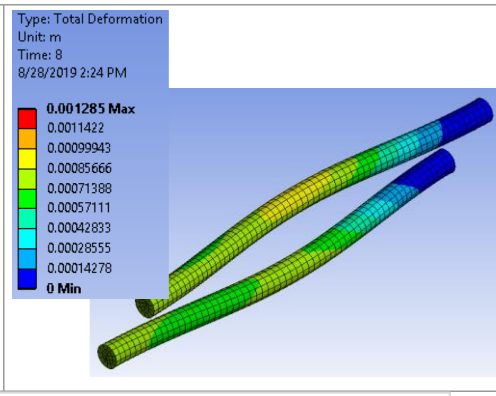
</td>
</tr>
<tr>
<td>Stress-Strain Curve compared with Reference curve from study by Wang et. al.</td>
<td colspan="2">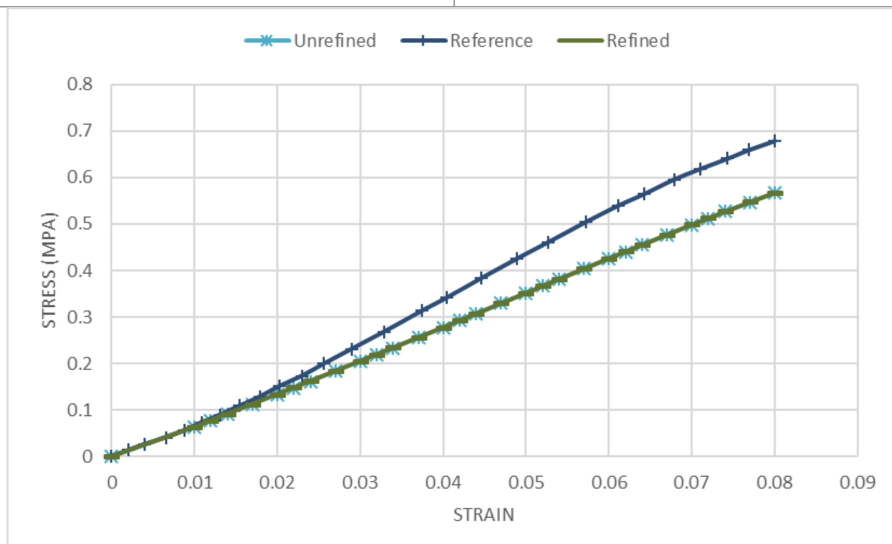
</td>
</tr>
</table>

Table 3 provides a comparison of a refined and unrefined mesh. Since the results show that the unrefined and refined mesh are the same, this shows that the simulations may be performed with less elements and faster simulation times. The simulation data is also compared with the results from related literature and shows that initial strain behaviour is similar upto 0.02 strain but start to diverge by upto a difference of 0.1MPa when it reaches 0.08 strain. This difference however is accepted as there may have been miniscule differences in meshing styles or material input from the simulations.

One of the major considerations for the future when implementing the metamaterial structure will definitely be the application on more realistic arterial shapes. Additional studies applying the structure right at bifurcation portion of the coronary must be taken into account as well since the structure will not be as simple as compared to applying the structure to just cylindrical portions of the arteries. The capability of the printer to print more accurately needs to be considered as well since the wave elements used in the simulations were already 0.6mm in diameter with their being a great possibly needing to further reduce the size if needed.

c. Comparison with experimental results

The results of the simulations were also compared with actual experimental results. The model used for the simulation was 3D printed and tested to a similar methods with the material property data gathering.

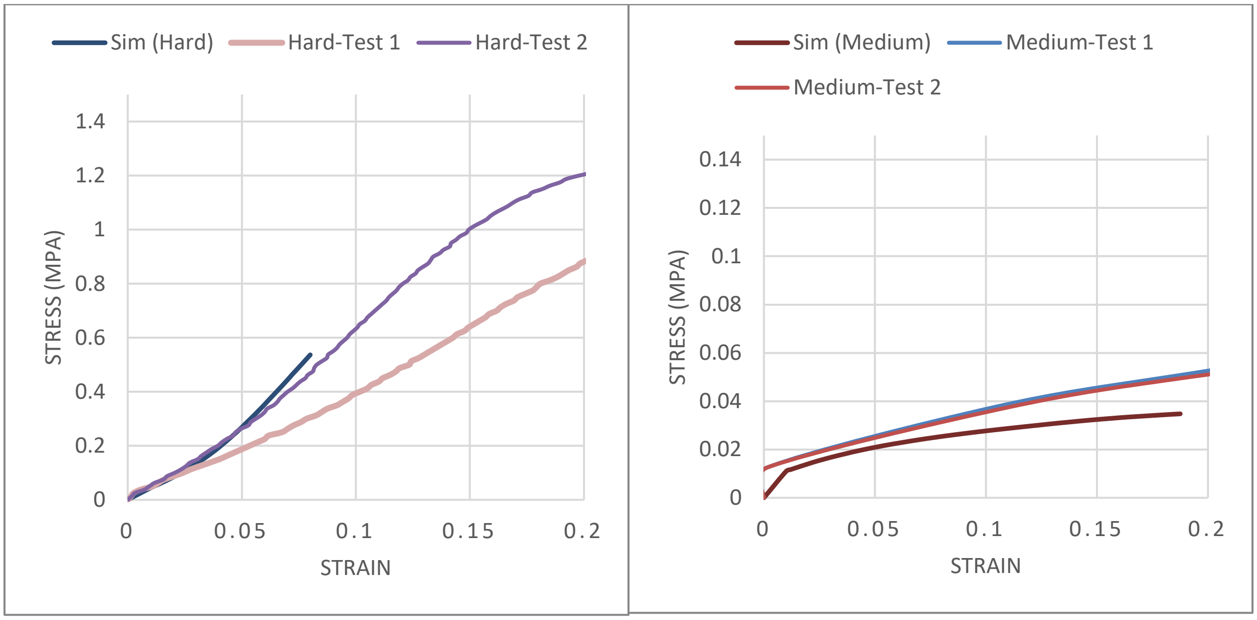

Figure 39. Curve comparison of Simulation results with Experimental Results.

As shown in Figure 39 and Figure 40, results from the experiment and simulations are similar values. The differences in the results may have been due to some human error discrepancies from the experimental set-up, material handling variables, or unknown printer variables. The results show similar modulus and trend and is therefore considered acceptable in this application.

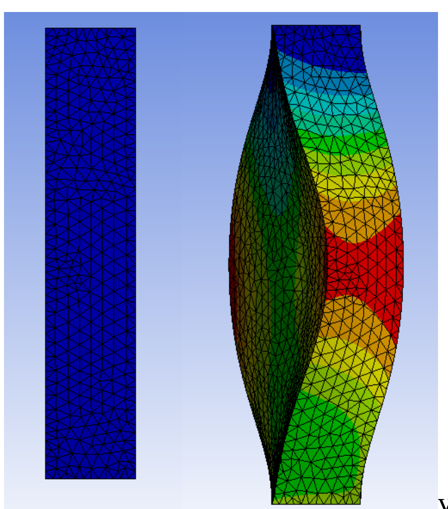
vs
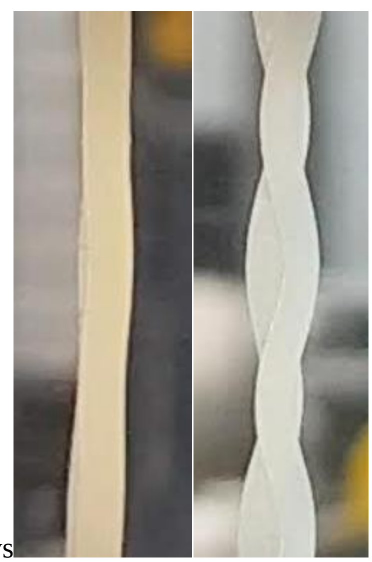

Figure 40. Deformation behavior of Simulation vs Actual at 8% stretch using a Hard material for the fibre

The deformation of the material from the simulation also showed a similar shape from the experiment when the samples are stretched to an 8% strain. This deformation behaviour however may be undesirable when applied to actual blood vessel phantoms and may therefore need to be considered for future studies to reduce the amount with methods such as scaling.

3. *Metamaterial Fibre Parameter Analysis*

The following sections show the results of changing a parameter while keeping the rest of the parameters constant. The results are compared with the target curve and values in Table 4 which is the Intima-axial or longitudinal from the study be Holzapfel et. al [15] Other than the parameter to be changed in each section, the base model's constant parameters are a fibre material of CL(hardest material), a fibre radius of 0.3mm and a fibre wavelength-to-amplitude ratio of 10mm:0.6mm. The modulus is calculated per 0.02 strain section while a %increase of the modulus from the previous section is provided as well.

Table 4. Target modulus and % increase

	Modulus E_n, MPa			
n	0	1	2	3
Target	0.54	0.69	1.15	2.01
% increase		28%	67%	74%

a. *Change in material*

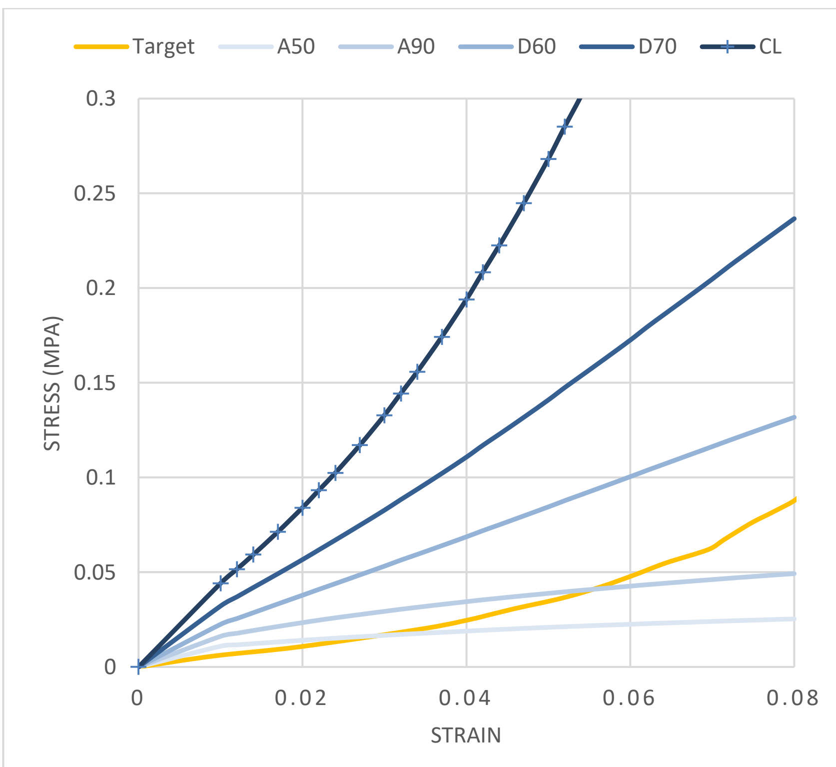

Figure 41. Effect of changing material

The effect of changing the fibre material is shown in Figure 41. In this scenario, the fibre shape is kept constant while the fibre material is changed from various stiffness levels. As expected, the material with the highest stiffness (CL) also results in a higher structure overall stiffness for the metamaterial.

Table 5. Effect of changing material on modulus

	Modulus E_n, MPa			
n	0	1	2	3
Target	0.54	0.69	1.15	2.01
% increase		28%	67%	74%
CL	4.20	5.50	7.95	9.18
% increase		31%	45%	16%
D70	2.83	2.71	3.09	3.20
% increase		-4%	14%	4%
D60	1.89	1.54	1.59	1.57
% increase		-19%	3%	-1%
A90	1.17	0.55	0.41	0.33
% increase		-53%	-26%	-20%
A50	0.70	0.24	0.18	0.14
% increase		-65%	-26%	-22%

In addition to an increased overall stiffness, the strain-stiffening behaviour of the structure becomes more evident as material stiffness is increased. As seen on the figure and table above, the increasing modulus signified by an increasing difference of stress relative to a constant strain increase shows a strain-stiffening behaviour. None of these however were able to significantly match the target. The only portion similar to the target was from using an A50 material upto a strain of approximately 0.02 from which it starts to diverge from the target since it does not reflect a strain-stiffening behaviour. This maybe due to the combination of the medium (A50) material being quite soft and its bonded contact with the matrix material.

b. Change in radius

The effect of changing the fibre radius is shown in Figure 42. In this scenario, the fibre material, wavelength and amplitude are kept constant. By decreasing the fibre radius, the overall stiffness of the structure decreases as well. The behaviour of the structure when changing the fibre radius is similar to the behaviour of changing the material.

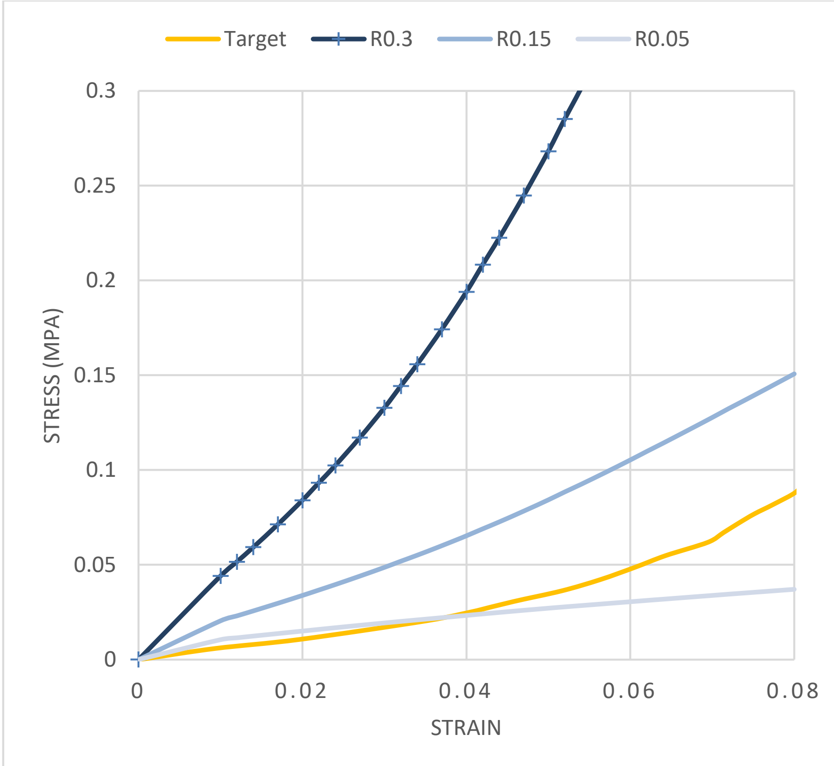

Figure 42. Effect of changing fibre radius

Compared from using the medium (A50) material from Figure 41 wherein the curve matches the target upto an approximate of 0.02 strain, the result of reducing the fibre radius to 0.05mm is closer to the target by a fraction since it is similar to the target upto an approximate strain of 0.04. Again similar to the change in material, the strain-hardening effect decreases as the overall stiffness also decrease.

Table 6. Effect of changing fibre radius on Modulus

	Modulus E_n, MPa			
n	0	1	2	3
Target	0.54	0.69	1.15	2.01
% increase		28%	67%	74%
R0.3	4.20	5.50	7.95	9.18
% increase		31%	45%	16%
R0.15	1.69	1.57	2.00	2.27
% increase		-7%	27%	14%
R0.05	0.75	0.41	0.36	0.33
% increase		-45%	-13%	-9%

c. *Change in amplitude and wavelength*

The effect of changing the wavelength to amplitude ratio is shown in Figure 43. The effect of the change in amplitude and the wavelength go hand in hand since it determines the straightness of the fibre. In this scenario, the material and fibre radius is kept constant. An increase in the wavelength to amplitude ratio results in the fibre forming more of a straight line aligned with the direction of the load. As a result, the higher ratio increases the stiffness of the structure.

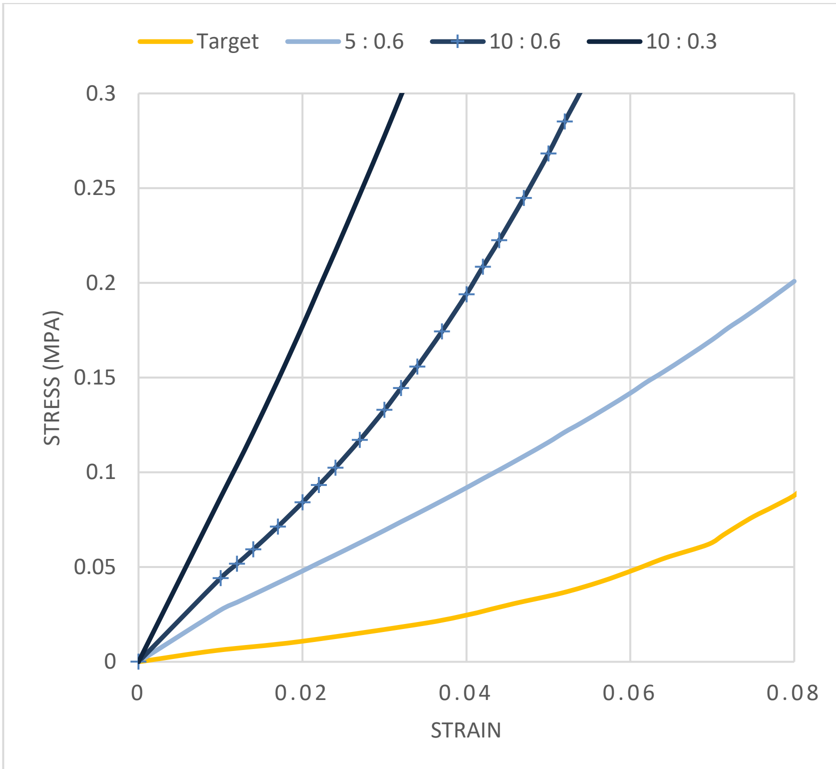

Figure 43. Effect of changing the wavelength to amplitude ratio

In contrast with the fibre material and radius change, the decrease in overall stiffness does not reduce the strain-hardening effect. In this case, when the overall stiffness is reduced, the %increase of the modulus increases to 18% for E_3 for a wavelength of 5mm and amplitude of 0.6mm.

Table 7. Effect of changing the wavelength to amplitude ratio on Modulus

	Modulus E_n, MPa			
n	0	1	2	3
Target	0.54	0.69	1.15	2.01
% increase		28%	67%	74%
5:0.6	2.40	2.20	2.50	2.95
% increase		-8%	14%	18%
10:0.6	4.20	5.50	7.95	9.18

% increase		31%	45%	16%
10:0.3	8.85	10.21	10.16	9.69
% increase		15%	0%	-5%

d. Change combination

In order to produce the strain-hardening effect at E_3, changing multiple parameters must then be necessary. For this combination, the radius of the fibre is 0.15mm while the wavelength is 5mm. The amplitude and material are kept the same as before. The effect of changing the radius and the wavelength to amplitude ratio is shown in Figure 44 along with with a comparison of changing just the radius and just to wavelength. In this case, it can be observed that the resulting curve decreased the overall stiffness again due to the combination of a reduced fibre radius and wavelength.

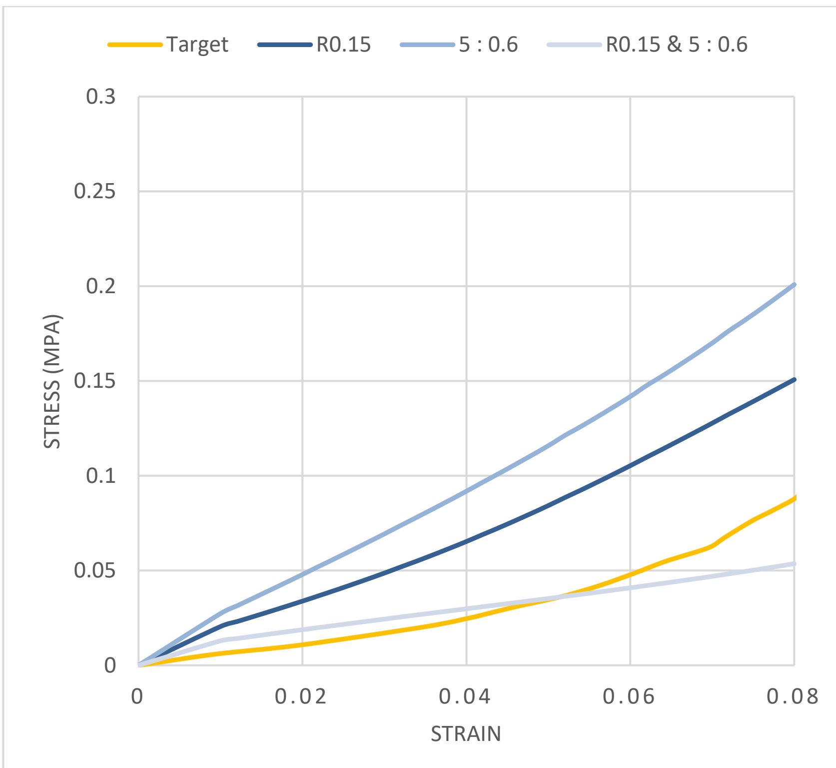

Figure 44. Effect of combining the change in radius and wavelength to amplitude ratio

Comparing the result of the combination with the result of just changing the radius to 0.05mm as shown in Table 8, it can be observed that a strain-hardening behaviour is more evident for the combination since the E_3 is reached a 15%increase compared to a decrease of 9% when only the radius was changed. However, the strain hardening behaviour of the target is still yet to be attained.

Table 8. Effect of combining the change in radius and wavelength to amplitude ratio on modulus

	Modulus E_n, MPa			
n	0	1	2	3
Target	0.54	0.69	1.15	2.01
% increase		28%	67%	74%
R0.15 & 5:0.6	0.94	0.55	0.55	0.64
% increase		-41%	0%	15%
R0.05	0.75	0.41	0.36	0.33
% increase		-45%	-13%	-9%

V. Limitations and Recommendations for Future Work

1. Additional Simulations and data verification & validations

To further this study, the 3D printing and simulations can be improved with additional verification and validating the results from performing studies such as:

- Horizontal specimens for tensile testing – for analysing the anisotropy of a 3D printed part
- Developing a structured mesh for simulations
- Exploring simulation methods other than kinematic hardening model for materials.

Additional simulations can be performed as well to determine the effects of different shapes and parameters such as:

- Effect of more parameter combinations.
- Effect of different shapes: sinusoidal, straight, double helix, interlocking chain, stent designs
- Application on realistic arterial shapes (patient specific scanned arteries)

2. Consultation with clinicians

For evaluation sample for clinicians, a more realistic model can be used. The model can be based from a scanned coronary artery with an applied thickness of at least 1mm. A disease shape can be modelled in Autodesk Inventor based on several shape and dimensions from several sources as can be seen on Figure 45. The disease is about 8mm long with a 50% stenting with a slight protrusion on the outer side of the vessel wall.

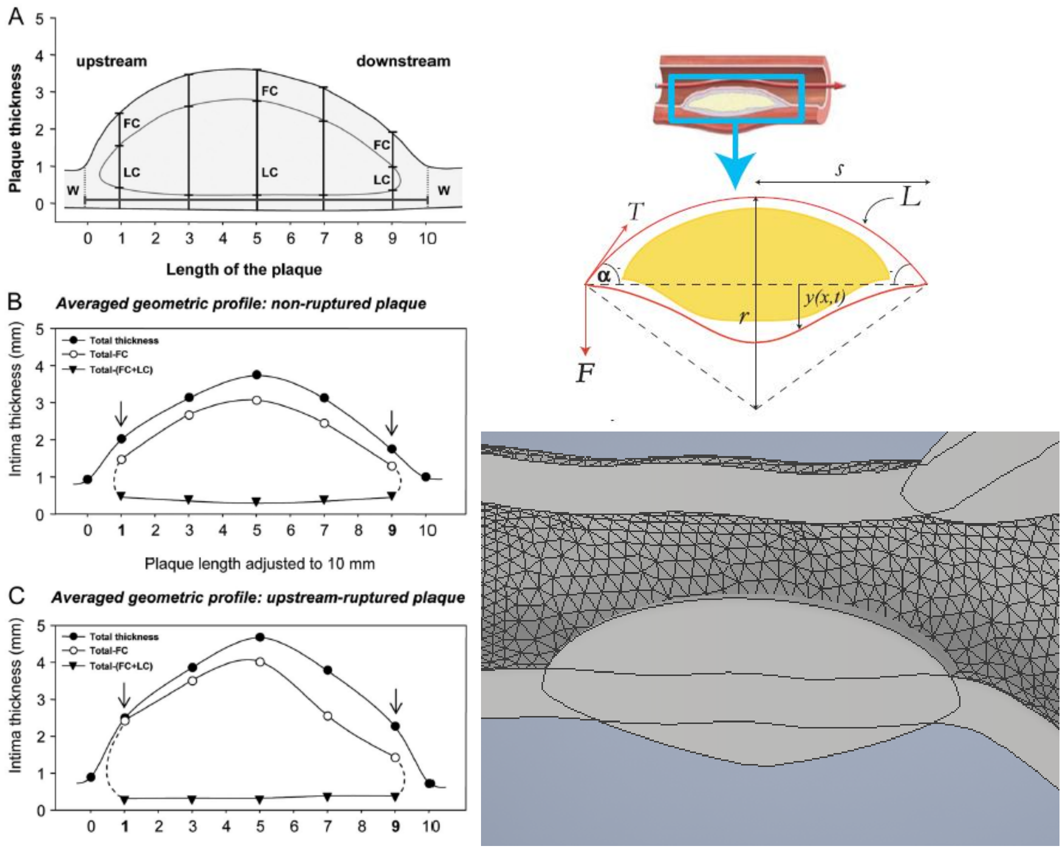

Figure 45. References for plaque geometry [33] [34] [35]

The 3D printing of the initial evaluation sample for clinicians can proceed for future study and shaped as shown below. A full body version is to be printed without the protrusion while the half model is printed with the protrusion of the disease as for evaluator to have a better feel of the part.

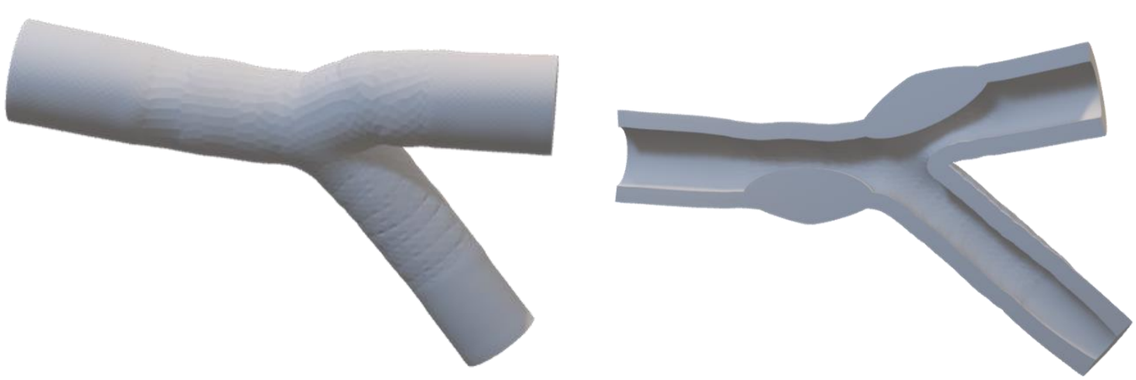

Figure 46. Full and Half body of the more realistic model geometry

VI. Conclusions

This study explored the feasibility of using a polyjet 3D printer, specifically the Projet MJP 5600 located in UNSW, to develop a realistic blood vessel replica that more accurately represents the mechanical properties of coronary arteries.

Using the available materials that can be used alongside the MJP 5600 printer and a two material (metamaterial) structure, the convex strain stiffening behaviour of a blood vessel tissue can be imitated. Fine tuning the design parameters are necessary to mimic the target stress-strain property with an increased accuracy. However, the design parameters of the metamaterial is limited to the 3D printer's printing size specifications and material selection. For this study, three design parameters for the metamaterial were investigated specifically the fibre's material, radius, and the wavelength to amplitude ratio. The effect of each are summarized as follows:

- Material – affects the overall stiffness of the structure. Stiffer fibre material will result in higher modulus.
- Radius – affects the overall stiffness of the structure. Lower fibre radii will result to lower modulus.
- Wavelength to Amplitude Ratio – affects the overall stiffness of the structure and affects the strain-stiffening behavior. A higher ratio will result to higher overall stiffness and less strain-stiffening effect.

While there is potential to accurately mimic the coronary artery tissue properties in future studies with metamaterials, the structure and available materials for this study however were unable achieve an exact replica of the stress-strain behaviour of the coronary artery and disease (plaque) as shown in comparisons from Figure 47 to Figure 50. For strains of less than 0.1, we can expect to find that it can be a good starting point for future studies as a number of previous studies indicate that blood vessels strain upto about only 0.05 along its circumference while assuming no deformation along its axis [29] [30] [31]. As for the hard and soft plaque, the properties of the hardest and softest MJP5600 3D printer material respectively are the closest in comparison.

It also important to consider that these coronary artery and disease properties will vary from each person. And with the continuous development of 3D printing technology and metamaterial design studies, there is a potential to create more accurate patient specific coronary artery replicas. Additionally, the metamaterial structures may also have applications to other fields where a specific mechanical behaviour is desired.

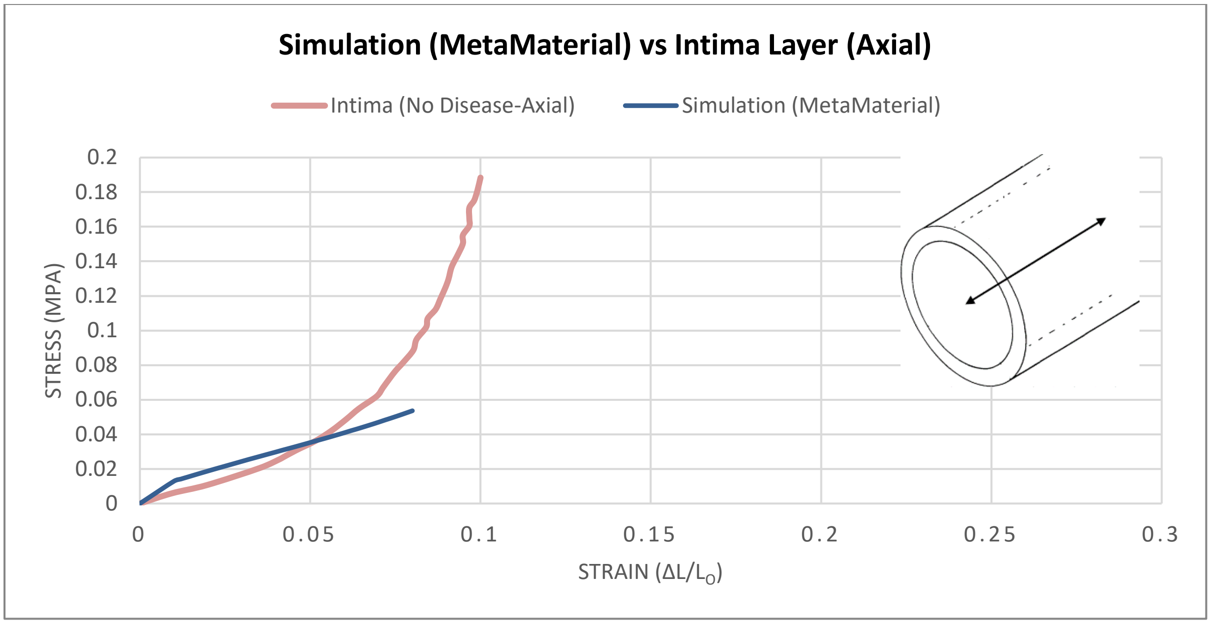

Figure 47. Metamaterial vs Intima Layer (Axial) Stress-Strain Comparison [15]

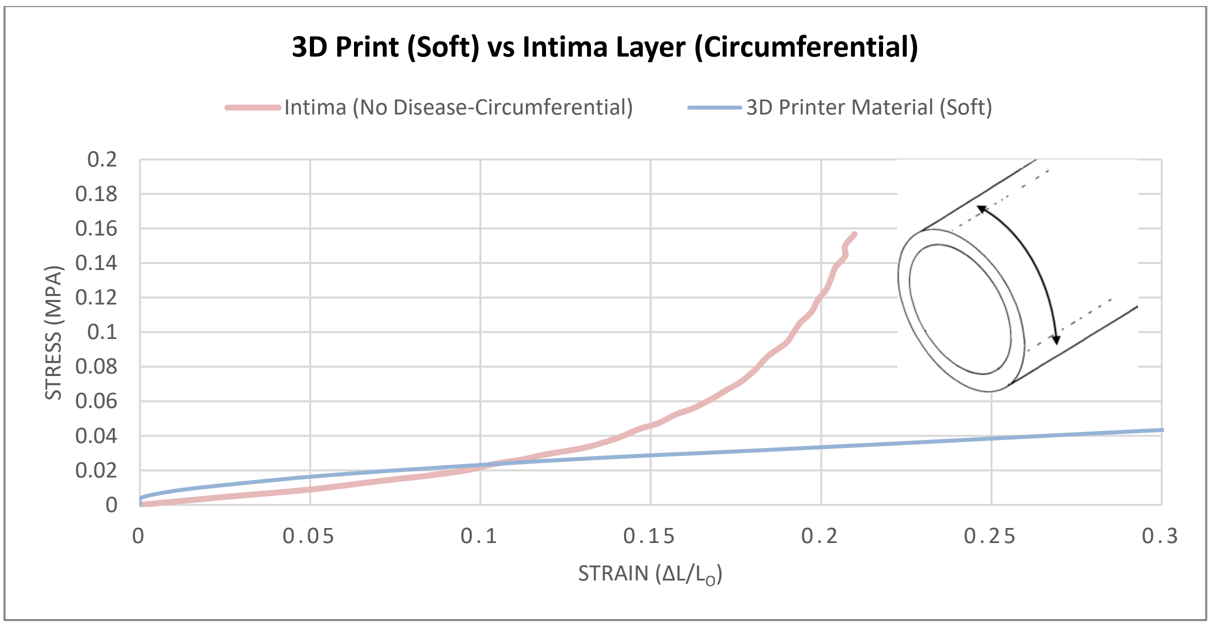

Figure 48. 3D Printed Soft Material vs Intima Layer (Circumferential) Stress-Strain Comparison [15]

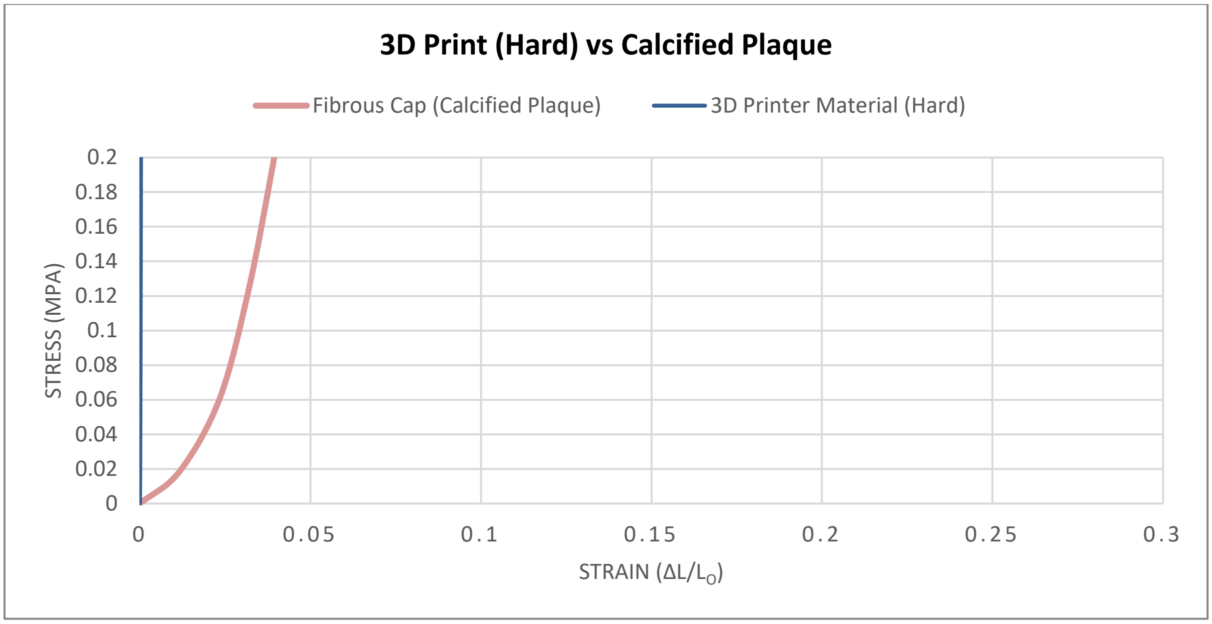

Figure 49. 3D Printed Hard Material vs Calcified Plaque Stress-Strain Comparison [16]

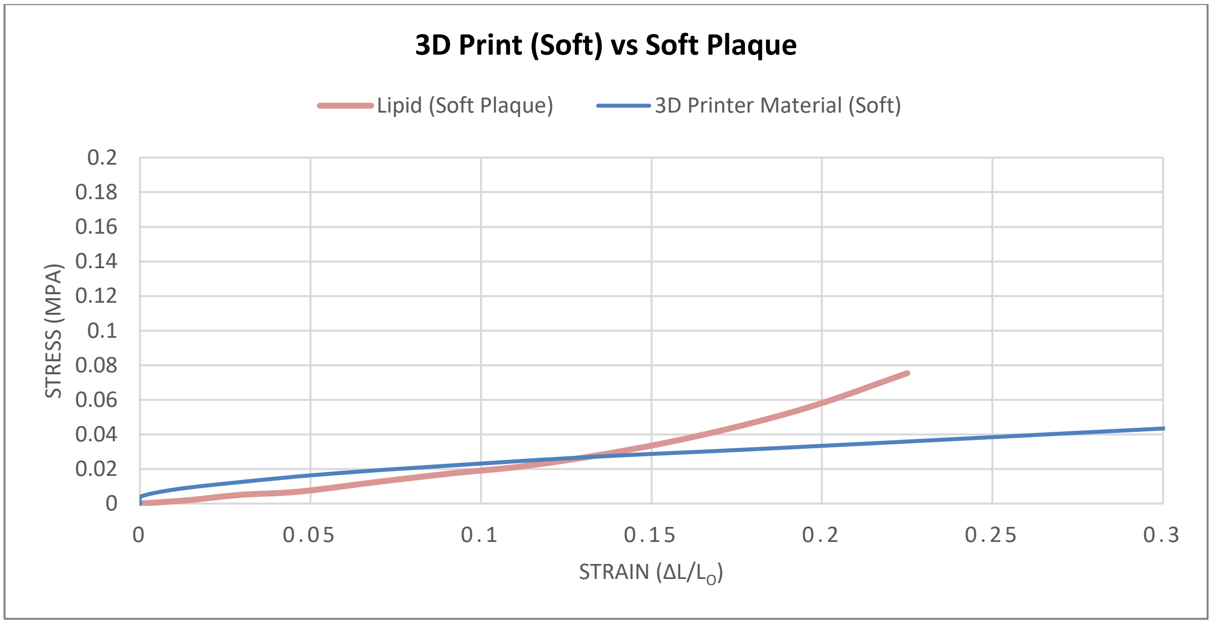

Figure 50. 3D Printed Soft Material vs Soft Plaque Stress-Strain Comparison [16]

References

[1] World Health Organization, "Cardiovascular diseases (CVDs)," [Online]. Available: https://www.who.int/news-room/fact-sheets/detail/cardiovascular-diseases-(cvds). [Accessed February 2019].

[2] "Heart disease fact sheet," [Online]. Available: https://www.heartfoundation.org.au/about-us/what-we-do/heart-disease-in-australia/heart-disease-fact-sheet. [Accessed February 2019].

[3] W. H. Organization, "Cardiovascular disease," [Online]. Available: https://www.who.int/cardiovascular_diseases/en/. [Accessed February 2019].

[4] A. Alwan, "Global status report on noncommunicable diseases 2010," World Health Organization, 2011.

[5] "What is coronary heart disease?," Heart Foundation, [Online]. Available: https://www.heartfoundation.org.au/your-heart/heart-conditions/what-is-coronary-heart-disease. [Accessed March 2019].

[6] "The progression of atherosclerosis," [Online]. Available: https://en.wikipedia.org/wiki/Atherosclerosis#/media/File:Endo_dysfunction_Athero.PNG. [Accessed February 2019].

[7] Heart Foundation, "Medical tests," [Online]. Available: https://www.heartfoundation.org.au/your-heart/living-with-heart-disease/medical-tests. [Accessed March 2019].

[8] Mayo Clinic, "Coronary artery disease," [Online]. Available: https://www.mayoclinic.org/diseases-conditions/coronary-artery-disease/diagnosis-treatment/drc-20350619. [Accessed March 2019].

[9] V. Filippou and C. Tsoumpas, "Recent advances on the development of phantoms using 3D printing for imaging with CT, MRI, PET, SPECT, and ultrasound," *The International Journal for Medical Physics Research and Practice,* 2018.

[10] J.Brunette, R.Mongrain, J.Laurier, R.Galaz and J.C.Tardif, "3D flow study in a mildly stenotic coronary artery phantom using a whole volume PIV method," *Medical Engineering & Physics,* vol. 30, no. 9, pp. 1193-1200, 2008.

[11] K. Wang, C.-C. Ho, C. Zhang and B. Wang, "A Review on the 3D Printing of Functional Structures for Medical Phantoms and Regenerated Tissue and Organ Applications," *Engineering,* 2017.

[12] 3D Systems, "ProJet MJP 5600," [Online]. Available: https://www.3dsystems.com/3d-printers/projet-mjp-5600. [Accessed April 2019].

[13] S. Bild, "SLA vs. PolyJet [Technology Review]," 14 August 2018. [Online]. Available: https://blog.trimech.com/sla-vs-polyjet-technology-review. [Accessed March 2019].

[14] VERYST Engineering, "ANISOTROPY OF 3D-PRINTED POLYMERS," [Online]. Available: https://www.veryst.com/project/Anisotropy-of-3D-Printed-Polymers. [Accessed March 2019].

[15] G. A. Holzapfel, G. Sommer, C. T. Gasser and P. Regitnig, “Determination of layer-specific mechanical properties of human coronary arteries with nonatherosclerotic intimal thickening and related constitutive modeling,” *AJP Heart and Circulatory Physiology,* 2005.

[16] G. A. Holzapfel, G. Sommer and P. Regitnig, “Anisotropic Mechanical Properties of Tissue Components in Human Atherosclerotic Plaques,” *Journal of Biomechanical Engineering,* vol. 126, pp. 657-665, 2004.

[17] L. H. Arroyo and R. T. Lee, “Mechanisms of plaque rupture: mechanical and biologic interactions,” *Cardiovascular Research,* vol. 41, no. 2, pp. 369-375, 1999.

[18] S. K. Nadkarni, “Optical measurement of arterial mechanical properties: from atherosclerotic plaque initiation to rupture,” *J. of Biomedical Optics,* vol. 18, no. 12, 2013.

[19] A. C. Akyildiz, L. Speelman, B. v. Velzen, R. R. F. Stevens, A. F. W. v. d. Steen, W. Huberts and F. J. H. Gijsen, “Intima heterogeneity in stress assessment of atherosclerotic plaques,” 2017.

[20] S. R. H. S. M. P. F. H. S. L. Z. Y. &. G. J. H. Barrett, “Experimental measurement of the mechanical properties of carotid atherothrombotic plaque fibrous cap,” *Journal of Biomechanic,* vol. 42, no. 11, pp. 1650-1655, 2009.

[21] C.-K. Chai, “Biomechanical properties of atherosclerotic plaques,” Technische Universiteit Eindhoven, 2015.

[22] Z. Teng, Y. Zhang, Y. Huang, J. Feng, J. Yuan, Q. Lu, M. P. Sutcliffe, A. J. Brown, Z. Jing and J. H. Gillarda, “Material properties of components in human carotid atherosclerotic plaques: A uniaxial extension study,” *Acta Biomaterialia,* vol. 10, no. 12, pp. 5055-5063, 2014.

[23] J. Singh, J. Depta and Y. Patel, “Bifurcation Lesions,” [Online]. Available: https://www.thecardiologyadvisor.com/home/decision-support-in-medicine/cardiology/bifurcation-lesions/. [Accessed March 2019].

[24] M. Watanabe, S. Uemura, Y. DOTE, Y. Sugawara, Y. Goryo, T. Ueda, H. Kawata and Y. Saito, “BIFURCATION ANGLE INFLUENCES ATHEROSCLEROTIC PLAQUE DISTRIBUTION IN CORONARY ARTERIES: AN OPTICAL COHERENCE TOMOGRAPHY STUDY,” *Journal of the American College of Cardiology,* vol. 63, no. 12, 2014.

[25] P. Chelladurai, W. Seeger and S. S. Pullamsetti, “Matrix metalloproteinases and their inhibitors in pulmonary hypertension,” *MATRIX METALLOPROTEINASES IN LUNG HEALTH AND DISEASE,* vol. 40, no. 3, p. 767, 2012.

[26] K. Wang, Y. Zhao, Y.-H. Chang, ZhenQian, C. Zhang, B. Wang, M. A. Vannan and M.-J. Wang, “Controlling the mechanical behavior of dual-material 3D printedmeta-materials for patient-specific tissue-mimicking phantoms,” *Materials and Design,* vol. 90, pp. 704-712, 2016.

[27] J. R. C. Dizon, A. H. E. Jr., Q. Chen and R. C. Advincula, “Mechanical characterization of 3D-printed polymers,” *Additive Manufacturing,* vol. 20, pp. 44-67, 2018.

[28] ASTM International, “D638-14 Standard Test Method for Tensile Properties of Plastics,” in *ASTM Standard*.

[29] D. Frakes and C. P. Cheng, “Arteries of the Head and Neck,” *Handbook of Vascular Motion,* 2019.

[30] E. O. Attinger, “The physics of pulsatile blood flow with particular reference to small vessels,” *Investigative Ophthalmology,* vol. 4, no. 6, p. 979, 1965.

[31] H. C. CHEN, V. PATEL, J. WIEK, S. M. RASSAM and E. M. KOHNER, “VESSEL DIAMETER CHANGES DURING THE CARDIAC,” *Eye,* vol. 8, pp. 97-103, 1994.

[32] K. Wang, C. Wu, Z. Qian, C. Zhang, B. Wang and M. A. Vannan, “Dual-material 3D printed metamaterials with tunable mechanical properties for patient-specific tissue-mimicking phantoms,” *Additive Manufacturing,* vol. 12, pp. 31-37, 2016.

[33] J. Bell, C. Breward, T. Chou, P.-W. Fok, J. M. Haugh, Q. Li, N. Mustafa, L. Rossi, A. Walter, X. Yang, A. Zemlyanova and N. Zhang, “Mathematical models for vulnerable plaques: MPI Workshop Delaware 2009,” 2009.

[34] P. Iwona Cicha, M. Anja Wo¨rner, M. Katharina Urschel, P. Kamen Beronov, P. Margarete Goppelt-Struebe, M. Eric Verhoeven, M. Werner G. Daniel and M. Christoph D. Garlichs, “Carotid Plaque Vulnerability. A Positive Feedback Between Hemodynamic and Biochemical Mechanisms,” *Stroke,* vol. 42, pp. 3502-2510, 2011.

[35] O. Ley and T. Kim, “Calculation of arterial wall temperature in atherosclerotic arteries: effect of pulsatile flow, arterial geometry, and plaque structure,” *BioMedical Engineering OnLine,* 2007.

Appendices

Appendix A. Gantt Chart

3D Printing Realistic Arterial Phantoms

UNSW
Fernan Bautista

: Start: Mon, 2/18/2019

Week: 1

TASK	START	END
Term 1		
Literature Review - Background	18/2	30/3
Project Plan - Methodology	18/3	17/4
Project Plan - Identify Additional Trainings Needed (Equipments)	1/4	1/5
Training	8/4	8/5
Term 2		
Premliminary Tests - 3D Printing & Testing	29/4	29/5
Testing and evaluations	27/5	25/8
Term 3		
Analysis	19/8	18/10
Final Report completion	7/10	6/12
Insert new rows ABOVE this one